AD-A123 897 DEFECTS IN AMORPHOUS METALS(U) HARVARD UNIV CAMBRIDGE MA DIV OF APPLIED SCIENCES F SPAEPEN JUL 82 TR-16 N00014-77-C-0002 1/1

UNCLASSIFIED F/G 20/12 NL

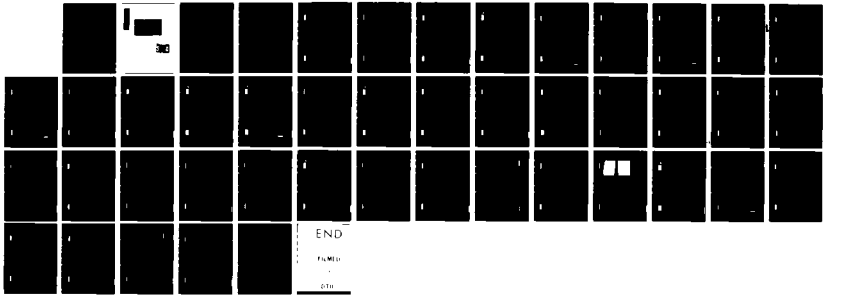

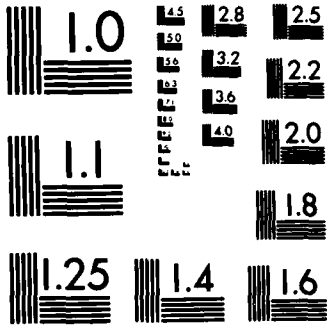

MICROCOPY RESOLUTION TEST CHART
NATIONAL BUREAU OF STANDARDS-1963-A

Office of Naval Research

Contract N00014-77-C-0002 NR-039-136

DEFECTS IN AMORPHOUS METALS

By

Frans Spaepen

TR 16

Technical Report No. 16

July 1982

The research reported in this document was made possible through support extended the Division of Applied Sciences, Harvard University by the Office of Naval Research, under Contract N00014-77-C-0002.

Division of Applied Sciences

Harvard University Cambridge, Massachusetts

Unclassified
SECURITY CLASSIFICATION OF THIS PAGE (When Data Entered)

REPORT DOCUMENTATION PAGE		READ INSTRUCTIONS BEFORE COMPLETING FORM
1. REPORT NUMBER Technical Report No. 16	2. GOVT ACCESSION NO. AD-A123897	3. RECIPIENT'S CATALOG NUMBER
4. TITLE (and Subtitle) DEFECTS IN AMORPHOUS METALS		5. TYPE OF REPORT & PERIOD COVERED Interim Report 6. PERFORMING ORG. REPORT NUMBER
7. AUTHOR(s) Frans Spaepen		8. CONTRACT OR GRANT NUMBER(s) N00014-77-C-0002
9. PERFORMING ORGANIZATION NAME AND ADDRESS Division of Applied Sciences Harvard University Cambridge, Mass. 02138		10. PROGRAM ELEMENT, PROJECT, TASK AREA & WORK UNIT NUMBERS
11. CONTROLLING OFFICE NAME AND ADDRESS		12. REPORT DATE July 1982 13. NUMBER OF PAGES 38
14. MONITORING AGENCY NAME & ADDRESS(if different from Controlling Office)		15. SECURITY CLASS. (of this report) Unclassified 15a. DECLASSIFICATION/DOWNGRADING SCHEDULE

16. DISTRIBUTION STATEMENT (of this Report)

This document has been approved for public release and sale; its distribution is unlimited. Reproduction in whole or in part is permitted by the U.S. Government

17. DISTRIBUTION STATEMENT (of the abstract entered in Block 20, if different from Report)

18. SUPPLEMENTARY NOTES

19. KEY WORDS (Continue on reverse side if necessary and identify by block number)

Amorphous metals; metallic glasses; defects; order-disorder; short-range order; free volume model; dislocations; atomic transport; diffusion; iso-configurational experiments; structural relaxation; creep; inhomogeneous flow; ductile fracture; brittle fracture.

1,000,000 K/s

20. ABSTRACT (Continue on reverse side if necessary and identify by block number)

"Amorphous metals" is a general term that refers to a class of solid metallic materials whose diffraction pattern shows no sharp reflections. When they are formed continuously from a melt by rapid quenching (usually around 10^6 K/s [1]) they can be called "metallic glasses." They can also be prepared by vapor, sputter, or electro-deposition, or even by ion-bombardment. Where the same metallic alloy has been prepared in amorphous form both by rapid quenching and by one of the other deposition techniques, the structure and many of the properties turn out to be rather insensitive to the method preparation.

DD FORM 1 JAN 73 1473 EDITION OF 1 NOV 65 IS OBSOLETE
S/N 0102-014-6601

Unclassified
SECURITY CLASSIFICATION OF THIS PAGE (When Data Entered)

COURSE 2

DEFECTS IN AMORPHOUS METALS

Frans SPAEPEN

Division of Applied Sciences,
Harvard University, Cambridge, MA 02138, U.S.A.

Contents

R. Balian et al., eds.
Les Houches, Session XXXV, 1980 – Physique des Défauts / Physics of Defects

1. Introduction

"Amorphous metals" is a general term that refers to a class of solid metallic materials whose diffraction pattern shows no sharp reflections [1]. When they are formed continuously from a melt by rapid quenching (usually around 10^6 K/s^{-1}) they can be called "metallic glasses." They can also be prepared by vapor, sputter or electro-deposition [2, 3], or even by ion-bombardment [6]. Where the same metallic alloy has been prepared in amorphous form both by rapid quenching and by one of the other deposition techniques, the structure and many of the properties turn out to be rather insensitive to the method of preparation [7].

The absence of sharp diffraction peaks is caused by a *lack of long-range translational symmetry*, and this is the only significance that should be attached to the term "amorphous." Therefore, in contrast with the etymology of the term, an "amorphous" structure can, in principle, be highly ordered. In most amorphous materials, a high degree of short-range order, i.e. a well-defined coordination number and distance, is usually established. However, it is possible to conceive of, and in some cases to approach experimentally, an amorphous structure which has long-range order. This simply means that the structure has a low configurational entropy, i.e. that the positions of all the atoms can be known from a small number of construction rules. There is no *a priori* reason why one of these rules must necessarily be translational symmetry. If an amorphous system could be obtained in equilibrium at absolute zero temperature, the third law of thermodynamics would require it to be fully configurationally ordered. We will refer to this, hypothetical, structure as the *ideal* amorphous structure.

In the first lecture, we will discuss the experimental evidence and the models for short- and long-range order in amorphous metals. Defects in these materials can be described as deviations from the ideal ordered structure. These deviations can be approached in two different ways:

(i) by considering what happens to ideal model structures when defects similar to point or line defects in crystals are introduced,

(ii) as local fluctuations of a thermodynamic property (such as the density, in the free volume approach).

The defects can then be classified according to the atomic transport function they perform.

In analogy with crystalline materials, we expect that in amorphous metals atomic transport processes, such as diffusion and plastic flow, are also governed by the formation and motion of defects. This will be the subject of the second lecture. In order to evaluate atomic transport measurements in amorphous metals properly, it is necessary to discuss first the fundamentally unstable thermodynamic state of these materials and their continuous relaxation towards metastable equilibrium. The experimental observations of atomic transport will then be critically reviewed, leading to some partial conclusions about the nature of the defects governing diffusion, homogeneous plastic flow and structural relaxation.

The third lecture will cover the remainder of the mechanical properties, namely the deformation processes at high stresses. When the stress on amorphous metal specimen becomes large enough, homogeneous plastic flow is superseded by a localized flow phenomenon: all the deformation becomes concentrated in a very thin shear band, and finally fracture occurs by a finger-like instability along the band. Under certain conditions of composition, temperature or annealing, however, this typical "ductile" fracture mode is not observed, and failure occurs at much lower stresses in a "brittle" mode. The phenomenology of all these processes will be surveyed and interpreted.

These lectures are not intended to be yet another review of the field of amorphous metals, since a number of very good and complete ones are available [1–5]. For this reason, the work that will be discussed should be regarded as collection of representative examples, and not as a complete survey of a very active field. Furthermore, since an understanding of the nature of structural defects in amorphous metals is only just emerging and is still very limited, some of the discussion of possible defect models will necessarily be rather speculative. It has been my intention to present, as much as possible, a unified point of view from which atomic transport and mechanical properties can be understood in a way that is consistent with our knowledge of the structure of these materials.

2. Structural order and disorder

2.1. Structural order

2.1.1. Short-range order (SRO)

2.1.1.1. SRO in amorphous pure metals. Some pure transition metals such as Co, Fe, Ni have been prepared in amorphous form by vapor deposi-

tion on a cold substrate [8]. A small amount (< 1%) of impurity is usually necessary for the crystalline temperature to be high enough for convenient observation. Diffraction studies of these materials [1] have shown that their structure is quite distinct from that of their respective crystalline form, not only because of the lack of long-range periodicity but also because of a fundamentally different SRO.

The structure of amorphous pure metals can not be described by an assembly of microcrystals, even if those are made very small or strained [9]. Rather, the model that gives the best fit to the radial distribution function is the dense random packing (DRP) of hard spheres with radius equal to the metal atom Goldschmidt radius. The DRP model, first constructed by Bernal [10] and later refined and characterized by Bernal and Finney [11], is obtained by physical maximum densification of a random assembly of hard spheres. It is completely amorphous in the sense that it has no translational symmetry, and has a well-defined density (14% less than that of the close-packed crystal). The initial characterization and more systematic later work by Frost [12] have shown that most of the polyhedra formed by connecting the centers of neighboring spheres are tetrahedra. This predominance of tetrahedral configurations is characteristic of the DRP and can be considered to be its fundamental difference with the crystalline structure: in a close packed crystal the ratio of tetrahedral to octahedral configurations is 2; in one of the studies of the DRP [13] this ratio was found to be 15.

The DRP, therefore, could be considered as the structure that maximizes the *local* density: the densest arrangement of four spheres is a tetrahedron; the densest packing of a few tetrahedra is five of them around a common edge; since fivefold rotational symmetry precludes translational symmetry, the resulting structure must be amorphous; since it is impossible to fill space with only tetrahedra without large distortions, some other polyhedra, such as octahedra, must also be present. The close packed crystal is, empirically, the densest possible arrangement of hard spheres, and can therefore be considered as the structure that maximizes the *overall* density. To achieve this, however, an octahedron must be incorporated for every two tetrahedra, which precludes the very dense local arrangements of the DRP.

This fundamental difference between the DRP and the crystal is also reflected in a fundamentally different SRO. Although the average number of nearest neighbors and the interatomic separation are very similar in both structures, the *angular* arrangement of the neighbors is different. This can be illustrated by considering a central atom surrounded by 12

touching neighbors. In the DRP, the ideal arrangement would be an icosahedral one (i.e. 20 tetrahedra sharing a vertex), where in the close packed crystal, it would be a cuboctahedral one (i.e. 8 tetrahedra and 6 half octahedra sharing a vertex). Although in both cases the number of neighbors and their distance to the central atom is the same, their angular distribution is fundamentally different. It may seem surprising that such a subtle difference in SRO could, by itself, lead to drastically different structures. However, the structure of amorphous Si or Ge is an even more striking example of this effect. In these materials, each atom has exactly four atoms at a well-defined nearest-neighbor distance, but a small change in angular SRO, (7° r.m.s. deviation of the bond angles from the ideal tetrahedral value of 109°) [14, 15] is sufficient to allow the construction of an amorphous random network, which is topologically completely distinct from the crystalline diamond cubic structure.

2.1.1.2. SRO in amorphous metal alloys. All of the amorphous metals produced by melt quenching are alloys. The largest and best characterized category are alloys of the type M_4X, where M is one or more of the transition or noble metals (Fe, Ni, Au, Pd, etc.) and X one or more of the metalloids (B, Si, P, etc.). Partial radial distribution functions, determined by X-ray or neutron diffraction on some of these binary alloys [16, 17], together with the partial coordination numbers obtained from EXAFS [18, 19] show that the chemical short-range order in the amorphous alloys is very high and that the coordination numbers and distances are almost identical to those in crystalline intermetallic compounds of similar composition. For example, the P-atom in both amorphous Ni_4P and crystalline Ni_3P is surrounded by 9 Ni-atoms and no P-atoms [16, 20]. Again, as pointed out in the previous subsection (2.1.1.1), the difference between the amorphous and crystalline phase derives from small differences in the angular arrangement of the metal atoms around the metalloid. This is illustrated in fig. 1 which shows some of the many different angular arrangements that can be made with 9 spheres (diameter = 1) surrounding a central one (marked +) at a distance 0.9.

Recently some attempts have been made to construct structural models for these alloys, by combining a relatively small number of fully ordered clusters, consisting of a metalloid atom surrounded by a number of metal atoms [21]. It remains an open question, however, whether such a model can be continued beyond a certain size without either lowering the density unrealistically, or relaxing the rigid SRO requirements of the

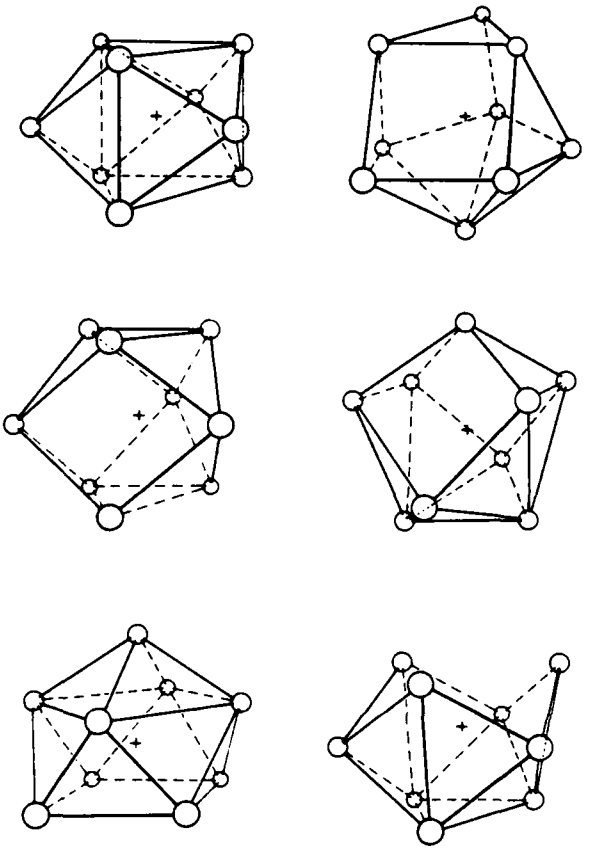

Fig. 1. Some of the possible angular arrangements for a constant coordination number (9 spheres of diameter 1 surrounding a central one, marked +) and a constant nearest neighbor distance (0.9).

cluster. The alternative approach has been to combine chemical SRO with the packing of hard spheres. The first suggestion along these lines was Polk's proposal of placing the metalloid atoms in the largest interstices of a DRP of metal atoms. Further developments of this approach have led to computer built binary hard sphere models, where the chemical SRO has explicitly been taken into account during the construction [22]. These models, can be made arbitrarily large and very dense; they fit the radial distribution functions well, but it is possible that their chemical SRO could still be improved.

There are many other compositional categories of amorphous alloys, such as the late–early transition metal alloys (Cu–Zr, Ni–Nb), the rare-earth-based alloys (Gd–Co), etc. The diffraction data for these alloys are not as complete as for the metal–metalloid alloys, but for some of them a high degree of chemical SRO has also been found [23].

2.1.2. Long-range order

In easy glass forming materials (organic compounds, polymers), the specific heat of the liquid can be measured at all undercooled temperatures. For these materials, the difference in entropy between the liquid and crystalline phase, ΔS_{fc}, can be determined and it decreases with increasing undercooling (see fig. 2). For amorphous metals, no measurements can be made in a temperature region between the glass transition temperature, T_g, and the melting point, T_M, because crystallization intervenes. However, a reasonable interpolation of the data results in a temperature dependence of ΔS_{fc} similar to that of the easy glass formers. However, ΔS_{fc} can strictly only be determined at temperatures where the liquid is still in internal (metastable) equilibrium; below the glass transition temperature, T_g, the time necessary for molecular rearrangements is long on the time scale of thermodynamic measurements, and the liquid (now a glass) can no longer be considered to be in internal equilibrium. Since the difference in specific heat between the glass and the crystal is small, the apparent (i.e. non-equilibrium) value of ΔS_{fc} does not change much below T_g (see dashed thin line in fig. 2), and gives a finite residual entropy difference ΔS_r at absolute zero. (This is not a violation of the third law of thermodynamics, since the system is not in internal equilibrium.)

The equilibrium value of ΔS_{fc} below T_g can only be estimated by extrapolation (see dashed heavy line in fig. 2). As pointed out by Kauzmann [86], this entropy difference seems to vanish at some finite temperature T_0. At this temperature, the amorphous phase would become fully configurationally ordered. We can only speculate about the nature of the ideal order in such an amorphous phase since it is experimentally totally inaccessible. Kauzmann interpreted the structural "catastrophe" at T_0 as a "spinodal crystallization" phenomenon: the amorphous phase would suddenly obtain long-range cyrstalline order. This interpretation, however, was based on the assumption that only translational symmetry could provide long-range order and on, now disproven, microcrystalline models of the liquid state.

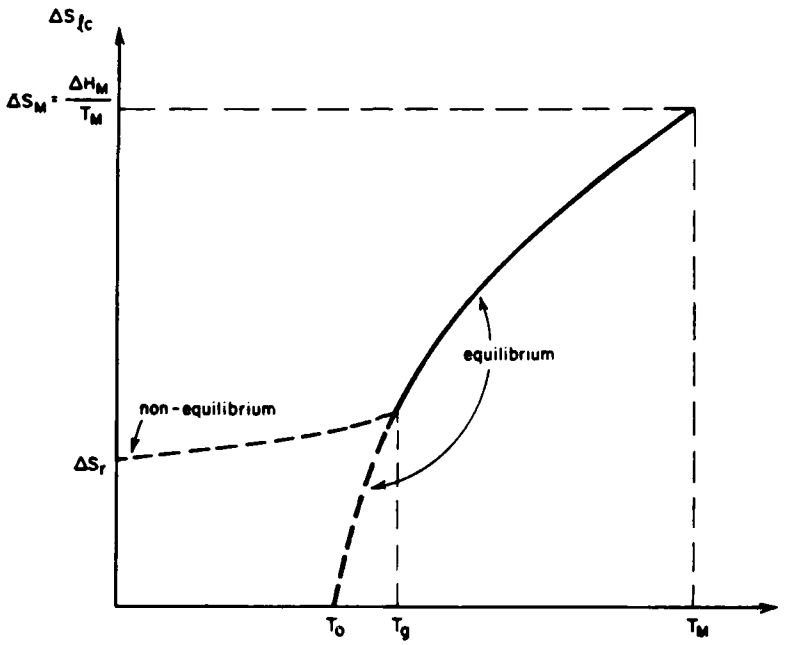

Fig. 2. Entropy difference, ΔS_{lc}, between the liquid (equilibrium) or glass (non-equilibrium) and the crystal as a function of temperature.

Our present knowledge about the distinct nature of the amorphous state and about the high degree of short-range order suggests a different interpretation. Some authors [24] have suggested that the DRP of hard spheres itself represents the equilibrium amorphous state at T_0. The topological constraints imposed by the densification of the system probably result in a low configurational entropy, but a precise calculation of this quantity would be very desirable. However, based on the same tetrahedral SRO as present in the DRP, it is possible to construct large amorphous hard sphere clusters that are obviously fully ordered [25].

It is of interest to note that the configurational entropy of a tetrahedrally coordinated random network is estimated to be quite low (< 0.2 k/atom) [26]. For this system, large ordered amorphous clusters have also been constructed. All these modeling studies seem to indicate that full configurational order can be achieved without translational symmetry. It remains to be demonstrated, however, that it can be extended to an infinite system.

2.2. *Structural disorder*

2.2.1. *Definition of defects*

In the previous subsection (2.1) we showed that the lack of translational symmetry, characteristic of amorphous materials, does not preclude a high degree of structural order. Therefore, we can define structural defects in these materials as local deviations from the ideal order. The simplest type of defects are deviations from the ideal chemical SRO – for example, pairs of P–P nearest neighbors in the amorphous Ni_3P alloy discussed above (subsection 2.1.1.2). Deviations from the ideal topological SRO are conceptually somewhat more difficult to approach, and they will therefore be the main focus of the following discussion. Since the experimental evidence about these defects is almost entirely indirect in nature (interpretation of atomic transport measurements), most of our knowledge about them comes from model studies.

2.2.2. *Modeling of defects from crystalline analogues*

One approach to the study of defects in amorphous systems is to introduce defects similar to crystalline point or line defects in highly ordered structural models and to observe their evolution and stability.

2.2.2.1. Vacancies. When a vacancy is introduced in an amorphous model system, e.g. by picking out a sphere in a two-dimensional dynamic hard sphere model [27] or by eliminating an atom during the molecular dynamics study of an amorphous cluster [28], it loses its identity very quickly by breaking up in small pieces which then get distributed throughout the system and finally disappear. This is, of course, quite different behavior from that of a crystalline vacancy, which remains localized and keeps its identity when it moves. A possible interpretation of this difference could be the availability of different types of energetically similar SRO arrangements in the amorphous system. This allows the system to distribute the defect as a number of small deviations from the ideal SRO, whereas the crystal, which has only a single type of SRO, must leave the vacancy as a topologically localized entity with, at most, some elastic relaxation. It might be of interest to note that the delocalization of vacancies has also been observed in some grain boundary models [29], where also a greater number of SRO arrangements exist than in the bulk crystal [30].

2.2.2.2. Dislocations. In their theories of the plastic deformation of amorphous metals, some authors have postulated the existence of generalized dislocations in these materials (Volterra dislocation with variable Burgers vector [31]; Somigliana dislocation [32]). These postulates were based on the macroscopic resemblance of the surface offsets produced during high-stress plastic flow of amorphous metals to the slip bands produced during plastic flow of single crystals. It has now been shown, however, that the surface offsets in amorphous metals are a result of localization of the plastic flow in shear bands [33, 74]; this is a macroscopic effect determined only by the constitutive flow law of the material (see subsection 4.2.2) for which it is not necessary to have microscopic dislocations.

The only attempt, so far, at modeling atom scale dislocations in amorphous metals has been the computer work of Chaudhari et al. [34]. They applied the continuum procedure for creating a dislocation to an amorphous monatomic cluster: a planar cut was made halfway down the cluster and one side of the cut displaced with respect to the other by a distance on the order of an atomic diameter; a displacement perpendicular to the end line of the cut produced an edge dislocation (i.e. material has to be added or removed), whereas a parallel displacement produced a screw dislocation. This initial configuration was then relaxed statically and the final configuration was examined by visual inspection and stress analysis. Their results showed that the edge dislocation was unstable and disappeared; the screw dislocation, on the other hand, seemed to be stable, in the sense that the final configuration contained its characteristic shear stress distribution. Some questions remain, however, on whether this kind of dislocation can be considered equivalent to a crystalline one, i.e. governing plastic flow. A molecular dynamics calculation would be useful to rule out the possibility of shallow metastability caused by the static nature of the relaxation procedure. It is also difficult to see how a screw dislocation could form, multiply or move without the presence of edge dislocations. A study of this defect under stress would therefore be instructive.

Very recently, Kobayashi et al. [35] have made a computer study of the high-stress deformation of an amorphous alloy model system. They observed localization of the plastic flow and from the residual stress pattern they concluded, qualitatively, that it occurred by the formation of a Somigliana dislocation. This is a very general type of defect, quite different from the screw dislocation described above. Their observations are limited, however, by the small size of their system. A more quantitative analysis of the stress field would also be desirable.

Direct experimental evidence of line defects in amorphous metals is difficult to obtain. The most convincing type of evidence, direct observation by electron microscopy, is ruled out by the absence of sharp diffraction peaks. Chen and Chuang [36] have performed positron annihilation experiments on amorphous metals before and after high-stress deformation. This technique can detect atomic scale "voids" such as vacancies and dislocation cores. Cold working of crystalline metals leads to a clear change in positron annihilation behavior, whereas no such change was observed in the amorphous metals. This argues against the existence of atomic scale dislocations in these materials. Recently Nold et al. [37] have performed small-angle neutron scattering on an as-quenched amorphous alloy and interpreted part of their data as scattering from the dilatational stress field of quenched-in edge dislocations. This seems to contradict the modeling work of Chaudhari et al. [34], unless the data can also be explained by other types of stress fields.

2.2.3. *Modeling of defects as structural fluctuations*

Although the conclusions of the previous subsection (2.2.2) are not entirely clearcut, it can still be stated that defects in amorphous materials differ in many ways from those in crystals. Both point and line defects seem to be more delocalized or "diffuse" in amorphous systems, and can therefore often be more fruitfully described as local fluctuations in the SRO than as generalized versions of localized crystalline defects. This approach is characteristic of most of the work that has been done on the transport properties of simple liquids and polymers. Depending on the property that is used to characterize the SRO, the fluctuations can be characterized in different ways.

2.2.3.1. Fluctuations in stress. Egami et al. [38] have analyzed the variations in the internal stress of computer-relaxed monatomic clusters, based on the DRP of hard spheres. They find variations on the scale of a few interatomic distances, in accord with another part of the neutron diffraction data mentioned above [37]. It is unclear, however, if these fluctuations are structural defects, in the sense that they deviate from the ideal SRO. It is known that atomic transport in the DRP is very slow [39, 40]. This means that the DRP, as discussed above (subsection 2.1.2), is a highly ordered amorphous structure with a very low concentration of defects. It is, therefore, very unlikely that any of these defects will be found in a small DRP cluster, which in turn means that they should not be identified with the reported stress fluctuations.

2.2.3.2. Fluctuations in configurational entropy. In this approach, originated by Adam and Gibbs [41] and recently applied to amorphous metals by Chen [42], the defect is defined as a subsystem that has a configurational entropy larger than some critical value, S_c^*, necessary to allow rearrangements. If the total configurational entropy of the system is known from thermodynamic measurements, the defect concentration can be calculated from fluctuation theory. This approach is inherently phenomenological. Its advantage is that atomic transport properties can be calculated from measurable thermal quantities. Its disadvantage is that it does not reveal the details of the defect motion on an atomic scale.

2.2.3.3. Fluctuations in density (free volume). This model, developed by Turnbull and Cohen [24], is in many respects equivalent to the previous approach (subsection 2.2.3.2), except that it is based on a specific atomic mechanism for defect rearrangement. If fact, the equivalency has been shown exactly in a limiting case [43]. In the free volume model for simple liquids, the DRP is considered to be the ideal amorphous state. The average atomic free volume, v_f, of a system is defined as the difference between its average atomic volume, v, and the average atomic volume of the DRP. It is assumed that the free volume can be redistributed among all the atoms without changing the energy of the system. If the local free volume of an atom becomes larger than some critical value, v^*, the atom can escape from its nearest neighbor "cage" and perform a diffusive or shear flow jump, i.e. it becomes part of a defect. In metallic systems, v^* is roughly equal to the volume of the metal ion core. The defect concentration, n, can then be calculated from the statistical distribution of the free volume among all the atoms:

$$n = \frac{1}{v}\exp\left(-\frac{\gamma' v^*}{v_f}\right), \tag{2.1}$$

where γ' is a geometric overlap factor of order unity. The simplest estimate of the temperature dependence of the free volume is $v_f(T) = \alpha v(T - T_0)$, where the coefficient of thermal expansion, α, is assumed constant. Since the viscosity, η, is inversely proportional to n, this gives $\eta = A\exp[B/(T - T_0)]$, where A and B are constants, which is the experimental Fulcher–Vogel type temperature dependence of the viscosity of simple liquids.

2.2.4. Classification of defects according to transport function

In crystalline materials, atomic transport is known to occur by the motion of defects. Vacancies govern diffusion and some form of creep:

dislocations govern high-stress deformation and, in combination with vacancies, some other forms of creep. Climbing dislocations and grain boundaries are also important as sources and sinks for establishing the equilibrium concentration of vacancies. Although the defects in amorphous metals are different from these crystalline defects, they must also perform the same basic transport function and can therefore be classified accordingly.

The basic feature in a diffusive atomic rearrangement is a change of nearest neighbors. It is clear how vacancy motion accomplishes this in crystals. An example of a "diffusion defect" that accomplishes this in an amorphous metal is the free volume fluctuation described above (subsection 2.2.3.3).

The basic feature of a "flow defect" is that, upon application of a shear stress, it undergoes a local shear transformation which is transferred elastically to the specimen boundary to produce macroscopic strain. Again, it is clear how the dislocation accomplishes this during slip in crystals. In an amorphous system, a free volume fluctuation can be a flow defect if, after the central atom's jump out of its nearest neighbor "cage", the collapse of the new "cage" around it produces a local shear strain. Although the original formulation of the free volume model involved only a single atom jump, it is straightforward to generalize the idea to involve the motion of several atoms, contained in a local defect volume v_0. When enough free volume is collected in v_0, the atoms can, under action of a stress, go through a shear transformation, and produce a local shear γ_0. This is illustrated schematically for a two-atom defect in fig. 3.

In order for a defect to be a sink for vacancies, it must be able to reverse the original vacancy formation mechanism; i.e. annihilation of the vacancy must result, through the elastic strain field of the defect, in a collapse inward of the specimen boundaries. Figure 4 illustrates how an edge dislocation functions this way for the annihilation of crystalline vacancies. The annihilation of "extra vacancies" or, more properly, "extra free volume" in an amorphous system is important during structural relaxation in the glassy state, where the system contains a non-equilibrium amount of free volume which is continually being annihilated until metastable equilibrium is reached (see below, subsection 3.1). A "relaxation defect" in an amorphous system can therefore be any site which, upon rearrangement after a free volume fluctuation, moves at least part of this volume elastically out to the specimen boundary. Such a site need not necessarily be the core of an edge dislocation. It could also be just a dilated region that can collapse down upon rearrangement. The

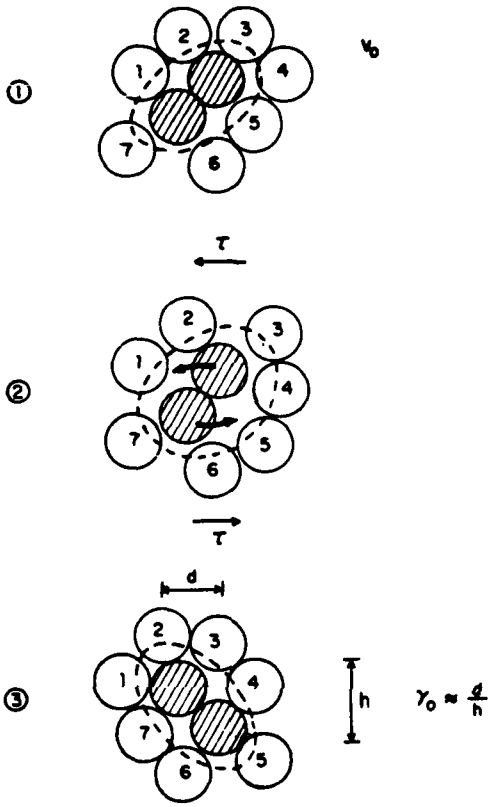

Fig. 3. Schematic diagram of the motion of a flow defect (volume v_0) under the action of a shear stress τ, producing a local shear strain γ_0.

equivalent of the collapse of a vacancy loop in crystals (see fig. 5) is also conceivable in amorphous systems. Since the criterion for the collapsibility of the loop depends, in the simplest analysis, on the ratio of the loop diameter and height, d/h, the breakup of vacancies in the amorphous state (subsection 2.2.2.1) could facilitate this process. In crystals, h can be no less than an interatomic distance λ. In amorphous systems, h can be less than λ, so that the total free volume that must be collected for collapse becomes much smaller ($\propto h^3$). This could account for the lesser degree of swelling observed during neutron irradiation of amorphous alloys, compared to that of their crystalline counterparts [44].

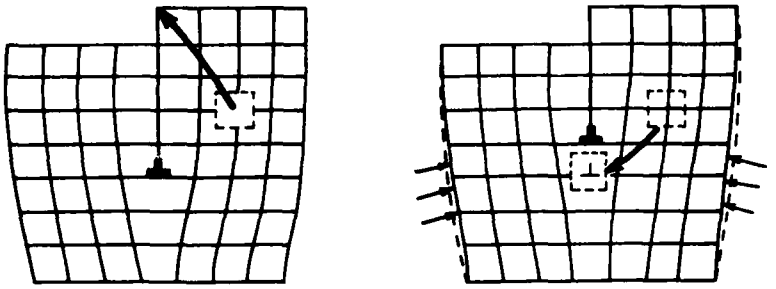

Fig. 4. Vacancy creation and annihilation processes in a crystal. Note the reversal of the volume change.

The rates of atomic transport during diffusion, flow or structural relaxation are often observed to be very different. Whereas earlier treatments often tended to ascribe all transport phenomena to the same defect, the distinction made above between "diffusion", "flow" and "relaxation" defects provides a straightforward qualitative explanation for possible differences in the respective transport rates. At the same time it should be noted that the categories can also overlap. The rearrangement shown in fig. 3, for example, contributes to both flow and diffusion.

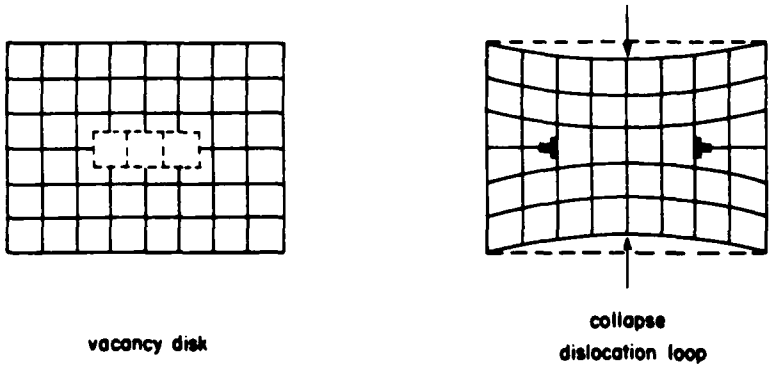

Fig. 5. Vacancy annihilation in a crystal by collapse of a vacancy disk and formation of a dislocation loop. Note the volume decrease.

3. Atomic transport properties

3.1. Isoconfigurational and equilibrium properties

As discussed above (subsection 2.1.2), the liquid phase is in stable equilibrium above the melting temperature, T_M, and in metastable equilibrium between T_M and the glass transition temperature T_g. Figure 6 shows, schematically, the temperature dependence of the shear viscosity, η, for a typical amorphous metal. The general shape of this curve is described by the Fulcher–Vogel type expression and is explained by the free volume model (subsection 2.2.2.3). At high temperatures ($T > T_M$) the free volume $v_f = \alpha v_0(T - T_0)$ is large and the defect concentration does not change very much with temperature ($\exp(\gamma' v^*/v_f) \to 1$). When T approaches T_0, however, v_f becomes small and the defect concentration decreases very rapidly, resulting in a sharp rise in the viscosity. In order to eliminate the defects, i.e. increase its structural order, the system must make configurational rearrangements. However, the rate at which these rearrangements can occur decreases as the order, and hence also the viscosity, of the system increases. Therefore, when the viscosity reaches a certain value the system will no longer have enough time to make the necessary structural rearrangement to come to equilibrium; it can be considered configurationally frozen. It is clear that the temperature at which this occurs, i.e. the glass transition temperature, T_g, depends on the time scale of the experiment or the quench rate of the sample. Typically, T_g is chosen to be the temperature at which the equilibrium viscosity is 10^{12} N s m^{-2}, which corresponds to an atomic jump frequency $k_\eta = kT/v\eta$ of 10^{-4} s^{-1} or one jump per hour. (See equation (3.7) for a derivation of k_η.)

When the configurationally frozen system is cooled below T_g, its viscosity still increases with decreasing temperature, but more slowly than if it had stayed in equilibrium. This can be interpreted most simply as follows [45]. The frequency with which an atom will perform a flow jump can be written as $k_\eta = (n_f v)k_f'$, where $(n_f v)$ is the probability that an atom belongs to a flow defect and k_f' is the jump frequency of an individual defect. Under *equilibrium* conditions, both n_f and k_f' decrease with decreasing temperature. Under *isoconfigurational* conditions (i.e. the system remains frozen), the viscosity rise upon lowering of the temperature only reflects the temperature dependence of k_f'. This analysis is somewhat oversimplified. A more detailed discussion will be given in

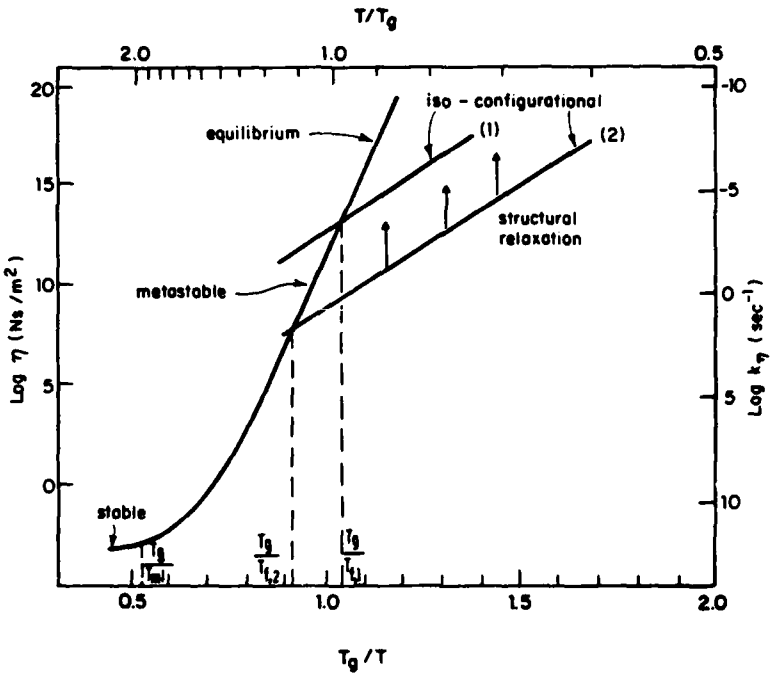

Fig. 6. Shear viscosity (η) and associated jump frequency (k_η) in the various stability regimes: stable equilibrium above T_M; metastable equilibrium up to T_g and extrapolated below; isoconfigurational (1) and (2) with associated fictive temperatures T_f below T_g. The direction of viscosity change due to structural relaxation towards equilibrium is indicated.

subsection 3.2.3. Figure 6 shows two isoconfigurational viscosity lines, corresponding to different quench rates.

If an amorphous system is left at a temperature above T_g, its viscosity does not change, because the system is in metastable equilibrium. Below T_g, the system is not in internal equilibrium, and therefore it relaxes continually towards the metastable state at that temperature. As a result, a continuous viscosity rise is observed at temperatures below T_g where there is some atomic mobility.

The structural state of a system below T_g is often characterized by its *fictive temperature* T_f, which was defined by Tool [46] as the temperature at which the structure of the system would be the equilibrium structure. Figure 6 shows how T_f can be determined from a knowledge of the isoconfigurational lines.

3.2. Homogeneous plastic flow

3.2.1. Review of the experiments

Homogeneous plastic flow in amorphous metals occurs at low stress levels. In this regime, every volume element of the specimen contributes to flow, in contrast with inhomogeneous flow, where all the deformation is localized in shear bands. When the homogeneous flow is Newtonian viscous (i.e. stress, τ, proportional to strain rate $\dot{\gamma}$), it can be characterized by the shear viscosity $\eta = \tau/\dot{\gamma}$. Figure 7 summarizes some typical data for a number of amorphous metals. Data obtained from viscometry (①) [47]) above T_M or from creep tests around T_g (② [48]) followed the equilibrium Fulcher–Vogel behavior. Early creep measurements below T_g (③ [49], ④ [50]) seemed to show that the temperature dependence of η was of the Arrhenius type with apparently a low activation energy. However, the structural relaxation phenomenon had not been taken into

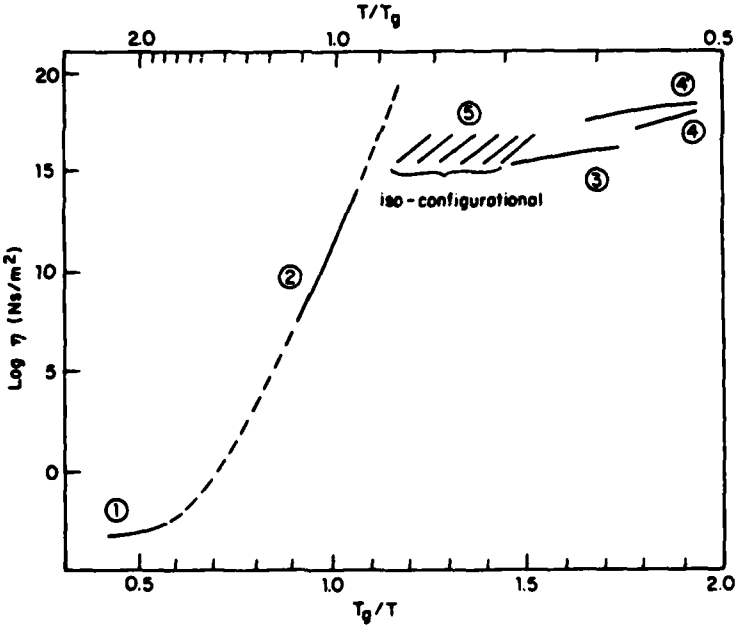

Fig. 7. Shear viscosity for a number of amorphous metals as a function of normalized inverse temperature. ① $Au_{77}Si_{14}Ge_9$ melt [47]; ② $Pd_{77.5}Cu_6Si_{16.5}$ equilibrium [48]; ③ $Pd_{80}Si_{20}$ not stabilized [49]; ④ $Co_{75}P_{25}$ not stabilized [50]; ④' $Co_{75}P_{25}$ not stabilized: rerun [50] and ⑤ $Pd_{82}Si_{18}$ isoconfigurational [51].

account in these tests. An indication of this was that a rerun of the set of tests ④ resulted in an increase in viscosity, as shown by the data ④'.

In order to obtain a physically interpretable activation energy, it is necessary to perform isoconfigurational experiments. For this, the system must be annealed for a long enough time, so that relative structural relaxation rate ($\mathrm{d} \ln \eta / \mathrm{d}t$), which decreases continually during annealing [51], becomes slow enough to allow measurements at different temperatures without appreciable structure changes. This can be checked by returning to the original annealing temperature and observing that no further viscosity change has occurred. The results of these isoconfigurational tests (⑤ [51]) show that the viscosity has an Arrhenius-type temperature dependence, at least within the T and η region of the tests, with a much higher activation energy (2 eV for $Pd_{82}Si_{18}$) than observed earlier. This means that structural relaxation during those early tests raised the viscosity at the higher temperature more than at the lower temperatures.

The data ⑤ also illustrate the very large increases in viscosity (up to 5 orders of magnitude) that can be obtained by annealing (up to 500 h in these experiments). In the same study [51] it was observed that the change of viscosity due to structural relaxation was *linear* in time when the specimen was annealed to change its structure between isoconfigurational measurements.

3.2.2. *Elementary theory of plastic flow*

For any system, subjected to a shear stress, τ, the plastic flow rate can be formulated most basically in terms of the general "flow defects" discussed above (subsection 2.2.4):

$$\dot{\gamma} = n_f \gamma_0 v_0 k_f, \tag{3.1}$$

where $\dot{\gamma}$ is the shear strain rate of the system, n_f the concentration of flow defects, v_0 the volume of one defect, γ_0 the local shear strain produced upon rearrangement of a defect and k_f the net jump frequency of a flow defect under the action of the stress.

The expression (3.1) is a completely general one, as can be seen, for example from its application to dislocation motion in crystals. Consider a crystalline system containing dislocations of average length, l, and with dislocation density ρ. The defect concentration is then $n_f = \rho/l$; the volume of the defect is that of a dislocation core $v_0 = \lambda^2 l$, where λ is the interatomic distance; the shear produced with the dislocation moves one lattice spacing $\gamma_0 = b/\lambda$, where b is the Burgers vector; the jump frequency

for dislocation motion can be expressed in terms of the dislocation velocity v_d: $k_f = v_d/\lambda$. This gives, in eq. (3.1): $\dot{\gamma} = \rho b v_d$, which is the well-known Orowan equation.

If no stress is applied, a defect can be considered to jump at an equal rate, k_f', between its forward (sheared) and backward (unsheared) position. When a stress is applied, these jumps are biased in the forward direction by a stress-dependent factor, $\beta(\tau)$. The net jump frequency of the defect under the action of the stress is thus:

$$k_f = k_f' \beta(\tau). \tag{3.2}$$

It is expected that k_f' would be of the form:

$$k_f' = k_a \exp(-\Delta G^*/kT), \tag{3.3}$$

where k_a is the attempt frequency ($\sim$ Debye frequency) and ΔG^* the activation barrier for motion (strain energy or chemical bond breaking energy). Since $\tau\gamma_0 v_0$ is the work done by the applied stress upon forward motion of the defect, it represents the difference in chemical potential between the forward and backward position. Simple rate theory [52] then gives an expression for the biasing factor as the difference of two fluxes of exponential form:

$$\beta(\tau) = \sinh\left(\frac{\tau\gamma_0 v_0}{kT}\right). \tag{3.4}$$

If the stress is small ($\tau < kT/\gamma_0 v_0$), the sinh can be equated with its argument and

$$\beta(\tau) = \frac{\tau\gamma_0 v_0}{kT}. \tag{3.5}$$

In this regime, the flow is Newtonian viscous, and a shear viscosity, η, can be defined:

$$\eta \equiv \frac{\tau}{\dot{\gamma}} = \frac{kT}{n_f(\gamma_0 v_0)^2 k_f'}. \tag{3.6}$$

The number of unbiased flow jumps *per atom* in the system, k_η, used above (subsection 3.1) can easily be derived from this by choosing a specific defect model. For example, in the simplest free volume approach, the defect is one atom, which jumps one interatomic distance. So $v_0 = v$ and $\gamma_0 = 1$. From (3.6) follows then:

$$k_\eta \equiv (n_f v) k_f' = kT/v\eta. \tag{3.7}$$

3.2.3. Discussion of the flow defect

The temperature dependence of the viscosity η is dominated by $n_f k_f'$ [see eq. (3.6)]. For the equilibrium viscosity, the Fulcher–Vogel type dependence can be explained quite well by the free volume model, through the temperature dependence of n_f. [See above eq. (2.1) and subsection (3.1).] As discussed above, in the isoconfigurational case one would, at first, expect n_f to be constant, so that the temperature dependence of η must be ascribed entirely to k_f'. This means, from eq. (3.3), that, for example in the case of $Pd_{82}Si_{18}$, $\Delta G^* = 2$ eV [51], which is a rather large energy for an activation barrier for motion. Furthermore, if the temperature dependence of k_f' is the same magnitude as that of n_f around T_g (compare the 2 eV activation energy for k_f' to the total 5–10 eV apparent activation energy for the equilibrium η), the product $n_f k_f'$ would no longer have a Fulcher–Vogel-type dependence, since k_f' has a simple Arrhenius-type dependence.

The only way this problem can be resolved is if n_f is not constant during the isoconfigurational experiments. In fact, v_f is not constant during those experiments, since the coefficient of thermal expansion is clearly non-zero below T_g. If this volume change, rather than just leading to a rescaling of the fluctuations without a change in their number, can be at least be partly redistributed to form a new free volume distribution, its influence on n_f can be considerable. Crucial to this, however, is that this redistribution be *reversible* and fast. Microscopically, these reversible readjustments could be described as slight adjustments in the atom positions, without drastic structural rearrangements or changes in chemical order. This is different from the *irreversible* changes accompanying structural relaxation, where free volume is being annihilated at an appropriate relaxation defect. As discussed above (subsection 3.2.1), this irreversible process is known to be much slower in nature, presumably reflecting the low concentration of relaxation defects. As a result, it is possible to do isoconfigurational measurements by performing them quickly enough to avoid appreciable further irreversible relaxation, while at the same time the viscosity of any point on the isoconfigurational line can be reproduced because of the fast reversible changes.

The existence of two mechanisms of volume change is reflected in the large increase in the coefficient of thermal expansion, α, at T_g. For example, in amorphous $Pd_{77.5}Cu_6Si_{16.5}$, α is twice as large above T_g than below [53]. This means that the drastic structural rearrangements associated with the irreversible relaxation below T_g can take place within the time allowed for the measurement of α, only above T_g.

A consequence of the proposed mechanism is that the viscosity would have a non-Arrhenius temperature dependence below T_g. Recent experiments in our laboratory have indeed shown that the isoconfigurational activation energy is substantially larger around T_g than in the temperature regime shown in fig. 7. More extensive measurements and development of a quantitative model of the isoconfigurationals are underway.

The results of creep measurements of the stress-strain rate relation are often, empirically, described by a power law:

$$\dot{\gamma} = C\tau^m. \tag{3.8}$$

All measurements shown on fig. 7 correspond to the Newtonian viscous regime ($m = 1$), but other workers have reported values as high as $m = 10$. However, recent measurements [54], performed on well-stabilized $Pd_{82}Si_{18}$ samples (no structural relaxation) in steady-state flow over a large stress range, have shown this to be a result of the expected (subsection 3.2.2) sinh-dependence of the strain rate on the stress. An analysis of the literature data also showed that the high exponents could be correlated well with the stress range of the tests. A fit of eq. (3.4) to the results of $Pd_{82}Si_{18}$ yielded a value for $\gamma_0 v_0$ of 48 Å^3, or a little more than 3 atomic volumes. This means that the flow defect can be either 3 atoms making a substantial ($\gamma_0 = 1$) rearrangement (as in a generalized version of the free volume model, fig. 3), or a larger defect producing a small local strain (as in Argon's model [74] for homogeneous flow). It is clear however, that a dislocation mechanism would not be appropriate. Since for a dislocation $\gamma_0 = b/\lambda \approx 1$, and $v_0 = \lambda^2 l$, the average dislocation length, l, would only be 3 interatomic distances. It does not seem to be very fruitful to consider the motion of such a contorted dislocation, consisting of many short segments. In this limit, it reduces to a set of local fluctuation-type flow defects.

3.3. Diffusion

3.3.1. Review of the experiments

Direct measurements of the diffusivity in amorphous metals require special sensitive techniques because, in order to avoid rapid crystallization, they have to be performed below T_g, and even at that temperature the diffusivity is only 10^{-20} m^2 s^{-1}. Only a few such investigations have been reported, all of them on transition metal–metalloid alloys. The results for the diffusivity of the transition metal atoms are shown in fig. 8. The first investigation ① was made by Gupta et al. [55] who

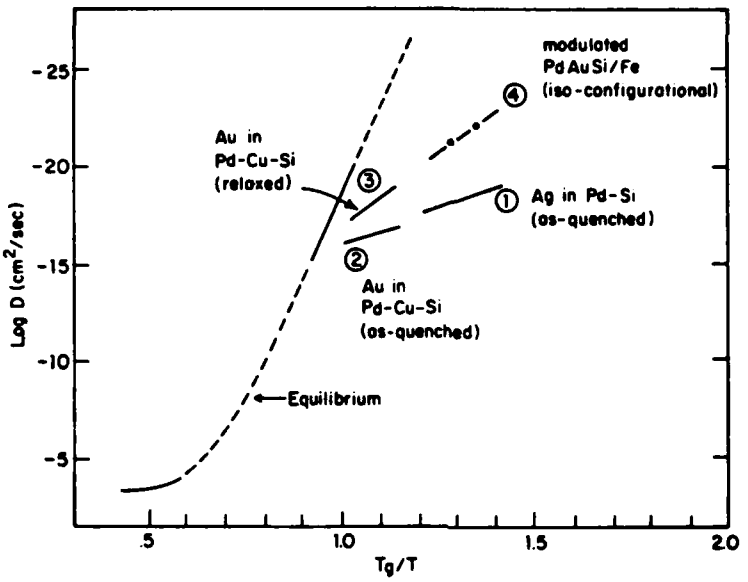

Fig. 8. Diffusivity of metal atoms in a number of amorphous metal–metalloid alloys: ① ^{110}Ag in $Pd_{81}Si_{19}$, not stabilized [55]; ② Au in $Pd_{77.5}Cu_6Si_{16.5}$, not stabilized [56]; ③ Au in $Pd_{77.5}Cu_6Si_{16.5}$, annealed [56] and ④ interdiffusivity in a $(Pd_{80}Au_7Si_{13})_{70}/Fe_{30}$ modulated film, isoconfigurational [57]. The equilibrium curve has been drawn by scaling the equilibrium viscosity curve (fig. 7) according to the Stokes–Einstein relation.

ion-implanted ^{110}Ag in $Pd_{81}Si_{19}$ and measured the broadening of its composition profile by sputter-sectioning. The temperature dependence of their results gave a low activation energy of 1.3 eV, similar to what had been observed in the early creep measurements. Since structural relaxation during the experiment had not been taken into account in this investigation either, the low activation is not physically meaningful.

And, exactly analogous to what has been observed in the creep experiments [51], stabilization of the structure by preannealing led to a large decrease in diffusivity and an increase in the activation energy. This was the work of Chen et al. [56], who determined the diffusivity of ion-implanted Au in $Pd_{77.5}Cu_6Si_{16.5}$ by measuring the broadening of its composition profile by Rutherford backscattering. Their results are shown in ② and ③. Data ② were taken on As-quenched samples, and exhibited the same low activation energy as ①. Data ③ were taken on samples preannealed around T_g. This results in a two order of magnitude

decrease in diffusivity and an increase in the activation energy to 1.67 eV. It seemed likely that these last measurements were isoconfigurational, but it had not specifically been checked.

The first controlled isoconfigurational experiment was performed by Rosenblum et al. [57]. They measured the interdiffusivity of compositionally modulated amorphous $(Pd_{80}Au_7Si_{13})_{70}/Fe_{30}$ sputter-deposited films by monitoring the decrease in intensity, I, of the satellite of the (000) X-ray scattering peak during isothermal annealing. This technique, developed by Hilliard and co-workers [58] for crystalline materials, is not only a very sensitive one ($\tilde{D} = 10^{-27}\,m^2\,s^{-1}$ can be measured), but it also allows a continuous check of the diffusivity, since at any time $\tilde{D}$ can be determined from the slope of a log I vs. time plot. The first data point of ④ was obtained by annealing for 127 h at the higher temperature (511 K). It was observed that $\tilde{D}$ decreased because of structural relaxation for many hours, and finally settled down at the reported value. The temperature was then lowered to 484 K and kept there for 168 h. No further structural relaxation was observed, and the second data point of ④ is therefore isoconfigurational with the first one. Significantly, these data agree well with an extrapolation of Chen et al.'s results after preannealing ③. The activation energy is 1.73 eV, which approaches the value of 2 eV for isoconfigurational creep [51] in $Pd_{82}Si_{18}$. It was also observed that the relative rates for changes in diffusivity ($-\tilde{D}^{-1}\,d\tilde{D}/dt$) and viscosity ($\eta^{-1}\,d\eta/dt$) were of the same order of magnitude.

Two sets of measurements of metalloid (or, more precisely, small atom) diffusion in these alloys have been reported. Birac and Lesueur [59] measured the diffusivity of Li in $Pd_{80}Si_{20}$ by ion implantation and neutron activation. Cahn et al. [60] measured the diffusivity of a sputter-deposited surface layer of ^{10}B in $Fe_{40}Ni_{40}B_{20}$ by secondary ion mass spectroscopy. In both cases, the reported diffusivities were several orders of magnitude higher than any of the reported metal diffusivities at the same normalized temperature, but no clear Arrhenius-type temperature dependence was observed. Since in both experiments the state of annealing of the specimens is unknown, a physically meaningful value of the activation energy could not be obtained. It is significant, however, that the boron results agree in magnitude with indirect determinations of the diffusivity from measurements of the rate of crystallization [61].

3.3.2. Scaling of diffusivity and viscosity

The diffusivity, D, can be calculated microscopically from the theory of the random walk. This gives

$$D = a_D k'_D \lambda_D^2. \tag{3.9}$$

where a_D is a dimensionless constant (of order unity) that takes into account the dimensionality of the system and the correlation of the jumps; k'_D is the diffusive jump frequency *per atom* and λ_D is the distance of a diffusive jump (expected to be on the order of an interatomic distance λ). If the concentration of diffusion defects is n_D and the jump frequency of a defect k_D, then:

$$k'_D = n_D v k_D. \tag{3.10}$$

Combining eqs. (3.9) and (3.10) with eq. (3.6) derived earlier for the viscosity gives:

$$\eta D = a_D \frac{n_D}{n_f} \frac{\kappa_D}{k'_f} \frac{\lambda_D^2 v}{(\gamma_0 v_0)^2} kT. \tag{3.11}$$

If there exists some relation between the flow and diffusion defects (for example if one defect performed both functions, or one type is a subset of the other), η and D are expected to scale with a characteristic length,

$$L = \frac{(\gamma_0 v_0)^2}{\lambda_D^2 v}. \tag{3.12}$$

For example, in the simple free volume picture (subsection 2.2.3.3) the same defect performs both functions. So, $n_D = n_f$, $k_D = k'_D$, $\lambda_D = \lambda$, $\gamma_0 = 1$, $v_0 = v \approx \lambda^3$. In this case $L = \lambda$ and

$$\eta D = a_D \frac{kT}{\lambda}, \tag{3.13}$$

which, for $a_D = 1/3\pi$, is the Stokes–Einstein equation.

An example of a process with a different scaling length is Nabarro–Herring creep in a polycrystalline sample subjected to a tensile stress σ (see fig. 9). In this mechanism of plastic flow, vacancies are injected into the grains at grain boundaries normal to the tensile axis; they diffuse through the grains and are annihilated at grain boundaries parallel to the tensile axis. This results in an elongation of the grains in the direction of the tensile axis. The basic expression for the shear strain rate, obtained by combining eqs. (3.1), (3.2) and (3.5) can be written the same way for uniaxial tension

$$\dot{\varepsilon} = n_f \varepsilon_0 v_0 k'_f \frac{\sigma \varepsilon_0 v_0}{kT}. \tag{3.14}$$

Combining eqs. (3.9) and (3.10) gives an expression for the diffusion coefficient

$$D = a_D n_D v k_D \lambda_D^2. \tag{3.15}$$

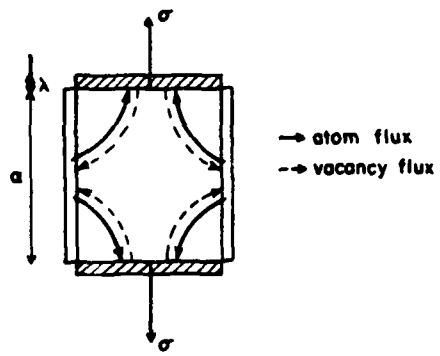

Fig. 9. Schematic diagram of the deformation and mass flux in a grain during Nabarro–Herring creep.

In Nabarro–Herring creep, the same defect (a vacancy) governs diffusion and flow; hence: $n_D = n_f$, $k_D = k'_D$ and $\lambda_D = \lambda$. The volume of the defect is the atomic volume: $v_0 = v$. If every atom in a grain performs *one* vacancy jump, the grain, of size d, increased in length by λ. The (tensile) strain per vacancy jump is then $\varepsilon_0 = \lambda/d$. So, using these quantities with eq. (3.15) in eq. (3.14) gives the well-known result [62]:

$$\dot{\varepsilon} = \frac{1}{a_D}\frac{D\sigma v}{kTd^2}. \tag{3.16}$$

The scaling relation (3.11) becomes now

$$\eta D = a_D \frac{kT}{L_{N\text{-}H}}. \tag{3.17}$$

with a scaling length $L_{N\text{-}H} = v/d^2$, which is much less than the interatomic distance found in the Stokes–Einstein relation.

If a scaling relation between η and D exists in amorphous metals, a determination of the scaling length, L [eq. (3.12)], can be of interest to determine the diffusional jump length λ_D, for example, if $\gamma_0 v_0$ has been determined from the stress–strain rate relation.

3.3.3. Discussion of the diffusion defect

All the present evidence seems to point to a great similarity between the diffusion defect and the flow defect.

In the liquid state ($T > T_M$), it is well known that the diffusivity and viscosity scale according to the Stokes–Einstein relation [eq. (3.12)]. Furthermore, as part of the diffusion experiments mentioned above,

Chen et al. [56] found this same relation to hold around T_g. For this reason, the equilibrium diffusivity curve on fig. 8 has been drawn by scaling the viscosity curve of fig. 7. As discussed above (subsection 3.3.2), the Stokes–Einstein relation follows most simply from ascribing both the flow and diffusion function to the same atomic scale defect.

It is also observed [45, 61, 63] that for most amorphous metals the activation energy for phase transformations, such as phase separation or crystallization, is close to the apparent activation energy of the viscosity at that temperature. Since in these amorphous alloys most phase transformations are diffusion controlled, this is another indication of the similarity between the flow and diffusion process.

The similarity in activation energy and structural relaxation rate of isoconfigurational creep and diffusion have already been pointed out above. Although a scaling relation between η and D in this regime is possible and seems likely, it has not yet been established completely. For this it is necessary to perform diffusion and creep measurements on *the same* stabilized specimen, to be sure that the degree of structural relaxation is the same for both experiments. However, given the scaling relation above T_g, one would not expect a drastic change in the flow defect upon going through the glass transition, and a continuation of the scaling relation seems therefore likely. The similarity in the rate of structural relaxation is also more easily explained if the flow and diffusion defect are both free volume fluctuations. If the flow defect were, for example, a dislocation, the relaxation process necessary to annihilate it would be very different from that necessary to annihilate a pocket of free volume.

The atomic rearrangements necessary for atomic diffusion seem to be very different from those necessary for structural relaxation. Experimentally, this is made most clear by the work of Chen et al. discussed above [56]. In order to produce observable broadening of the compositional profile, each atom in their samples must make at least 300 diffusive jumps. However, it is immediately clear from fig. 8, that the resulting diffusivities are still orders of magnitude larger than those at equilibrium at the same temperature. This means that the rate of structural relaxation can become much slower than the rate of atomic diffusion. In fact, it is a necessary condition for isoconfigurational experiments to be feasible at all. The simplest microscopic explanation for the difference in the diffusion and relaxation rate would be that the concentration of diffusion defects in the system is different from the concentration of relaxation defects. Considering that a diffusion defect requires only a switch of nearest neighbors, whereas a relaxation defect must have the appropriate

elastic stress field to annihilate free volume, a difference in their concentration is not implausible.

3.4. Conclusion

In summary, atomic transport experiments seem to indicate a similarity, if not identity, of the flow and diffusion defects, but a very distinct nature of the relaxation defects.

The flow and diffusion defects are probably rather localized, and can best be described as free volume fluctuations that allow, at the same time, a nearest-neighbor switch and local shear, as illustrated in fig. 3.

The relaxation defects are different, since they require long-range elastic stress fields for the irreversible annihilation of free volume. As a result, the rate of structural relaxation can become slow enough to permit isoconfigurational experiments.

In order to explain the large activation energies for isoconfigurational creep and diffusion, the idea of fast reversible structural relaxation below T_g has been introduced.

4. Deformation at high stresses

4.1. Deformation mechanism map

The plastic flow behavior of a material can conveniently be summarized by means of a deformation mechanism map – an idea first proposed by Ashby [64] and developed, for crystalline materials, by Ashby and Frost [65]. The axes of the map are normalized shear stress, $\log(\tau/\mu)$ (μ: shear modulus), and normalized temperature, T/T_M. On this map contours of constant steady-state shear strain rate, $\dot{\gamma}$, are shown using an appropriate superposition of the constitutive laws, $\dot{\gamma}(\tau, T)$, of all possible deformation mechanisms. Regions in which each of the mechanisms dominates are outlined. The validity of the respective constitutive laws can be checked by comparing this map with a similar plot of the experimental data.

An experimental deformation data map for Pd-based amorphous alloys is shown in fig. 10. In the light of what has been said above about the effect of structural relaxation of flow, such a map should only be drawn for specimens in the same state of annealing. This is obviously not the case for fig. 10, but it can still give a qualitative idea about the different regimes of deformation. From approximate contours of con-

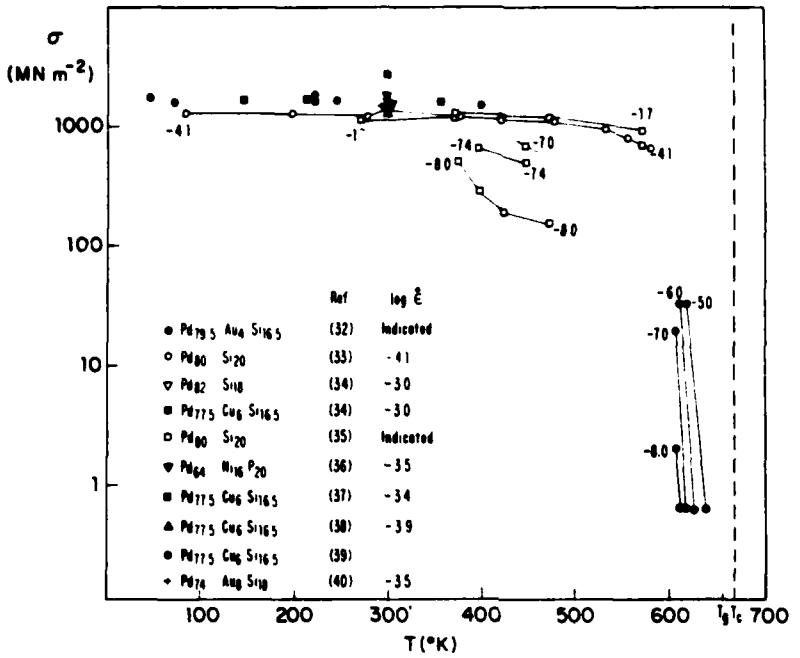

Fig. 10. Deformation mechanism data map for Pd-based amorphous metals (from ref. [33]).

stant strain rate drawn through the data, and from observations of the modes of deformation, an idealized deformation mechanism map for an amorphous metal in a well-specified state of annealing can be composed, as shown schematically in fig. 11. Two basic modes of deformation can be distinguished: homogeneous and inhomogeneous flow.

In homogeneous flow, as discussed in the previous subsection (3.2), each volume element of the specimen contributes to the strain. This mechanism operates at low stresses and high temperatures. The strain contours on fig. 11 reflect the shape of the equilibrium/isoconfigurational viscosity curves discussed above (see, e.g. figs. 6 and 7). As a result, the specimen gets longer and thinner uniformly, and fracture occurs after extensive plastic flow, when some part of the specimen has necked down to a small cross-section.

In the inhomogeneous flow regime the strain is localized in a number of very thin shear bands. As shown on fig. 11, this deformation mode operates at high stresses and lower temperatures. It will be the subject of the discussion in the following subsection.

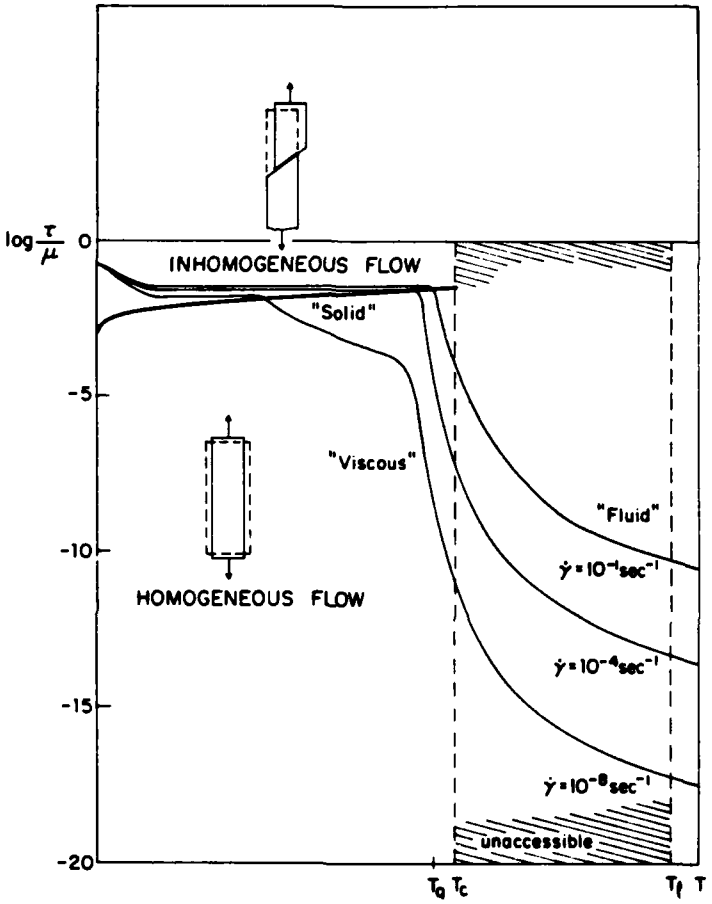

Fig. 11. Schematic deformation mechanism map for an amorphous metal (in a given state of annealing), illustrating the temperature and stress regimes for the two modes of plastic deformation (from ref. [33]).

4.2. Inhomogeneous plastic flow

4.2.1. Phenomenology

Inhomogeneous plastic flow occurs when amorphous metals are deformed at lower temperatures ($T < 0.7T_g$) in a tensile test, bending test or in a forming operation, such as rolling or wire drawing. The most striking feature about amorphous metals in this flow regime is their very

high strength [66]: they flow at shear stress levels of $\mu/50$, a value approaching the ideal shear strength of crystalline metals [67].

The strain rate contours in the inhomogeneous flow region of fig. 11 are spaced closely together and are almost horizontal, illustrating that the strain rate is very stress sensitive ($m = \partial \ln \dot{\gamma}/\partial \ln \tau$ is large; $m = 30$ has been measured for $Pd_{80}Si_{20}$ [68]) and almost temperature independent. For Fe-based alloys, a substantial increase in the flow stress is observed at very low temperatures [69].

The formation and propagation of a shear band is a rapid process [70] which is illustrated in fig. 12 for a ribbon pulled in tension. The band nucleates at a surface stress singularity, such as an edge crack (fig. 12a); it propagates through the specimen at 45° angle with the tensile axis (fig. 12b); after the band extends through the entire specimen, the two halves shear off uniformly (fig. 12c), which decreases the local cross-section until the stress concentration causes fracture to occur. The local plastic strain in a shear band is very high, since the two halves of the specimen shear off by a significant fraction of the specimen cross-section. The total macroscopic plastic strain, however, is much smaller ($\gamma = 0.002$), since there are usually only a few bands present in a tensile test. If a larger macroscopic strain is required (for example in a 180° bend of a ribbon), a large number of shear bands, as many as are required to produce the imposed strain, are generated.

The fracture surface morphology is shown in fig. 13a and illustrated schematically in fig. 13b. It is significant that the fracture occurs *along the shear band*, and not through the smaller cross-section normal to the tensile axis. The "vein" pattern displayed by the fracture surface morphology is typical of the instability that develops when two solid surfaces containing a fluid layer are pulled apart. (See also subsection 4.3.1.)

This type of fracture indicates strongly that the shear band consists of amorphous material that has undergone a structural change, which produces local *softening* (i.e. lowering of the viscosity). This obviously tends to concentrate all the deformation in the band and weakens it against failure by the mechanism described above. Differential etching [71] and electron microscopy observations [72] also indicate certain remanent structure changes in the band after removal of the load.

4.2.2. Microscopic description

The surface steps produced by the shear bands in amorphous metals (see figs. 12 and 13) are macroscopically reminiscent of the slip bands formed during plastic flow of crystals. As discussed above (subsection 2.2.2.2),

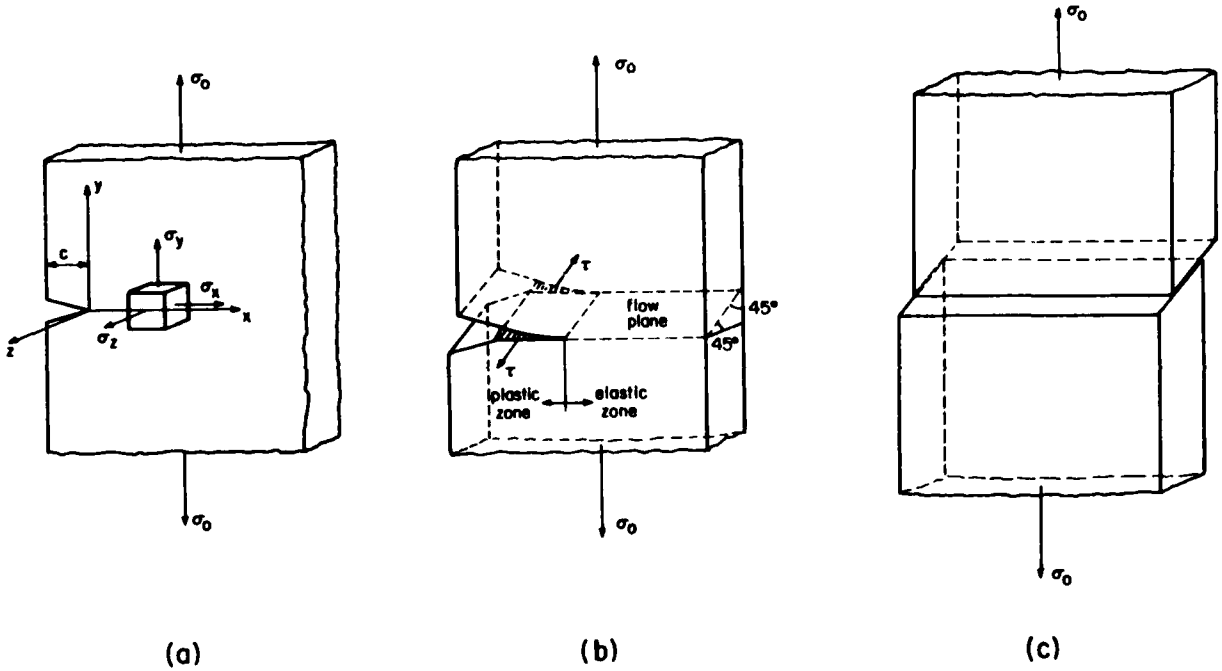

Fig. 12. Mechanics of the shear band motion in an amorphous metal ribbon under tension: (a) nucleation at an edge crack; (b) propagation through the specimen and (c) steady-state motion after passage of the singularity.

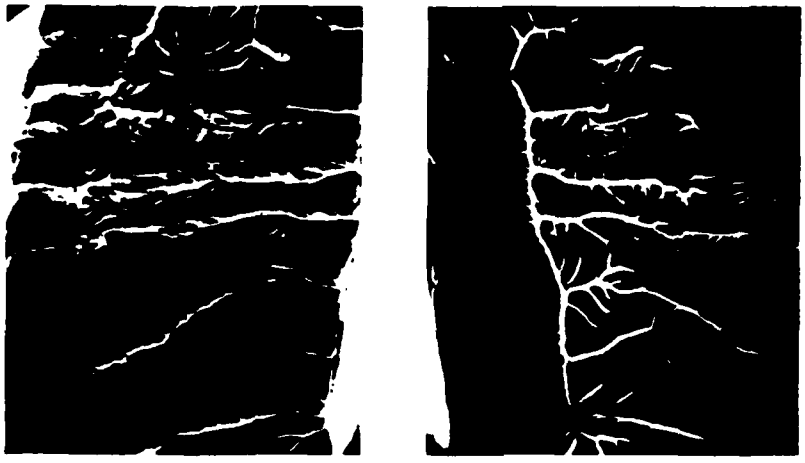

(a)

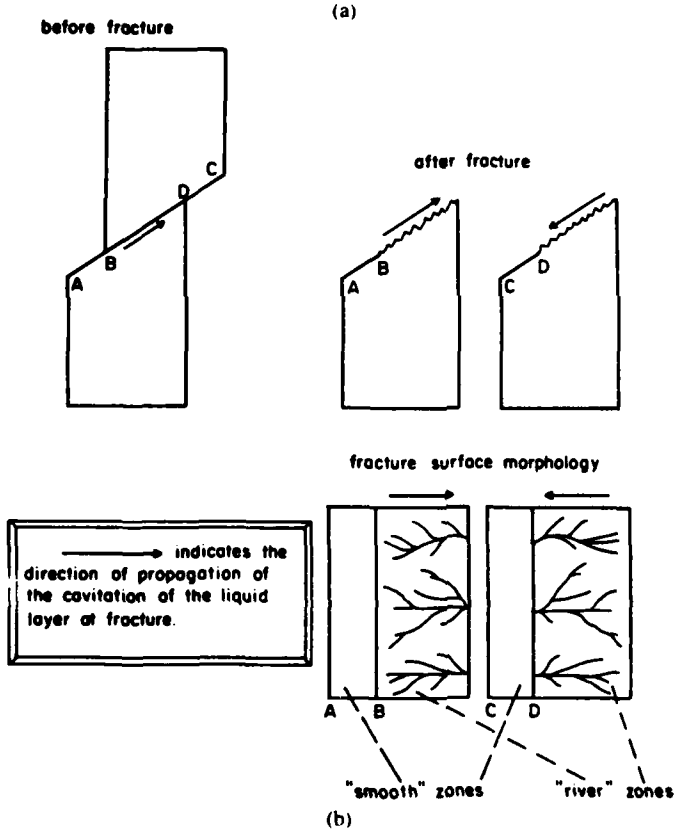

(b)

Fig. 13. (a) SEM observation of the matching fracture surfaces of an amorphous metal ribbon broken in the ductile fracture mode. (b) Diagram explaining the origin of the features of (a) and their relation to the shear band motion.

this has prompted some authors [31, 32] to invoke the existence of localized crystal-like dislocations to explain the inhomogeneous flow phenomenon. As discussed above, there are problems of a conceptual nature and of experimental verification with this type of dislocations. The approaches that use them also do not explain the localization phenomenon or the fracture surface morphology. The approach presented here is more in line with our present knowledge about the defects, as explained in the previous sections.

Spaepen and Turnbull [73] have proposed that the nucleation of the shear band at a surface crack is caused by the dilatation at the crack tip. They made an estimate of the negative hydrostatic pressure component of the triaxial stress state at the crack tip and concluded that it is large enough to cause a substantial dilatation, and hence an increase in the free volume. Since the viscosity is very sensitive to even small changes in free volume, the dilatation results in a dramatic viscosity drop at the crack tip. As a result, the material can flow locally on a 45° plane, since this corresponds to the direction of maximum shear stress. The high strength of the amorphous metals can be attributed to their ability to "blunt" cracks by this flow mechanism, rather than breaking by cleavage at a much lower macroscopic stress. The original stress concentration then propagates through the specimen at the tip of the moving shear band (fig. 12b), causing the softening mechanism described above to repeat itself.

After the stress concentration has passed through, the viscosity in the shear band remains low because of *strain disordering*: the localized flow destroys the structural order of the material in the band and hence lowers its viscosity; as long as the specimen is being deformed, this process keeps on disordering the material faster than it can be restored by structural relaxation.

This concept, first introduced by Polk and Turnbull [47], has been made more quantitative by Spaepen [33] by linking it up with the free volume theory. In this model, the disordering process is one of creation of extra free volume, as a result of atoms pushing their neighbors aside at a high enough stress; it is balanced by an ordering process similar to the structural relaxation described in homogeneous flow, during which the extra free volume is annihilated. When the creation and annihilation rates are equal, a steady state dynamic excess of free volume is established. This results in a higher flow defect concentration, n_f, given by:

$$\ln n_f = -\frac{\Gamma v^*}{2kTa}\left[\cosh\left(\frac{\pi v}{2kT}\right) - 1\right]^{-1}. \tag{4.1}$$

where $\Gamma = 2\mu(1 + \nu)/3(1 - \nu)$ is an elastic constant; and a is the number of jumps necessary to annihilate an amount of free volume equal to v^*. Notice that in the inhomogeneous flow regime the defect concentration is set by stress itself, as opposed to in the homogeneous regime, where it is set by the composition and the thermal history of the specimen.

Since n_f is a very strong function of τ, this model predicts a high stress sensitivity of the strain rate ($m = 50$). The boundary line between the homogeneous and inhomogeneous flow regions on the deformation mechanism map can also be accounted for if it is assumed that a is a number between one and ten. This is in accordance with model observations of vacancy annihilation in these systems (see subsection 2.2.2.1). However, since the rate of viscosity change due to structural relaxation has since been measured experimentally [51], the model should be adapted to take these relaxation results into account.

Using a creation and annihilation process very similar to the one described above, Argon [74] has analyzed the dynamics of shear band formation and shown that the localization is a direct result of the softening caused by the excess free volume.

4.3. Fracture

4.3.1. Ductile fracture

Ductile fracture is defined as the failure process, described above, following the formation of a shear band. The typical vein pattern of the fracture surface indicates that fracture occurs by an instability in the motion of the interface between the low-viscosity (fluid) layer and the air. This phenomenon was first described by Taylor [75] for the case of immiscible liquids, and was applied to this fracture phenomenon by Spaepen [76] and Argon and Salama [77].

An approximate analysis [78] of the phenomenon can be made as follows (see fig. 14). Consider a coordinate system associated with shear band, such that the plane of the band is in the xy-plane, and the air-fluid interface is in the xz-plane. The external tensile stress maintains a negative hydrostatic pressure inside the band. Since the pressure outside the specimen can be considered zero, the interface is driven inward by a negative pressure gradient $\partial p/\partial y$. Consider now an arbitrary sinusoidal perturbation of the interface:

$$y = \epsilon \sin(2\pi x/\lambda). \tag{4.2}$$

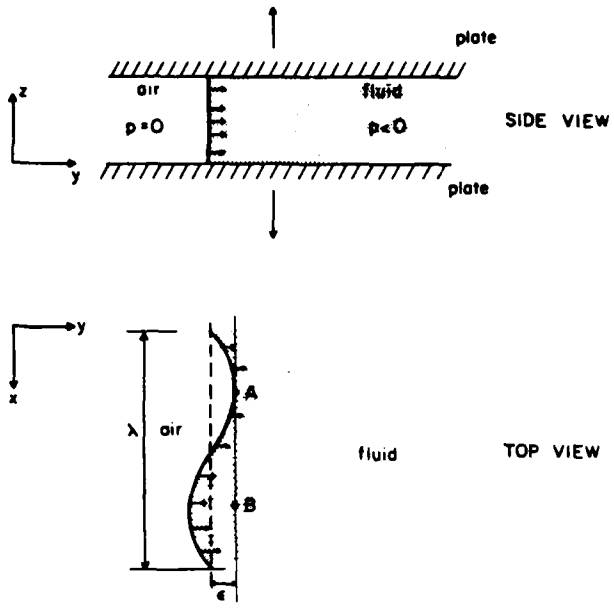

Fig. 14. Geometry and stress state of a fluid layer between two solid plates being pulled apart. See text for a discussion of the stability of the perturbation of wavelength λ.

At point A, just inside the fluid, the pressure, p_A is determined by the local curvature of the interface, κ, and the surface tension, γ.

$$p_A = -\gamma\kappa. \tag{4.3}$$

From eq. (4.2), the maximum curvature can be calculated,

$$p_A = -\gamma\epsilon(2\pi/\lambda)^2. \tag{4.4}$$

At point B, it is assumed that the influence of the surface curvature is not felt, and that the pressure, p_B, is simply determined by the original driving gradient:

$$p_B = -\epsilon|\partial p/\partial y|. \tag{4.5}$$

If p_A is less than p_B matter will flow from B to A and the perturbation will die out. If the reverse is true, matter will flow from A to B, and the perturbation will grow as a finger-like protrusion into the fluid. These fingers will eventually run into each other, and the material that piles up between them will, upon separation, produce the typical vein pattern.

The minimum wavelength, λ_c, for growth of a perturbation corresponds then to the condition $p_A = p_B$. This gives

$$\lambda_c = 2\pi\sqrt{\gamma/|\partial p/\partial y|}. \tag{4.6}$$

The wavelength that is observed on the fracture surface, however, corresponds to the wavelength that grows most quickly, λ_m. It can be found by adapting the perturbation theory of Mullins and Sekerka [79] for dendrite formation during crystal growth, which is a mathematically exactly similar problem (surface tension vs. temperature or concentration gradient). This gives $\lambda_m = \sqrt{3}\lambda_c$. Inserting appropriate values for the surface tension and the pressure gradient produces good agreement with the observed initial vein spacings.

4.3.2. Brittle fracture

The ability of amorphous metals to blunt cracks by localized flow and formation of shear bands is crucial to their high strength. Under certain conditions, however, these materials become brittle, i.e. they break by a cleavage mechanism. Empirically, this is often measured by a bending test: the material is called ductile if a ribbon can be bent back onto itself. The degree of brittleness can then be related to the minimum radius of curvature in such a test [66].

Amorphous metals can embrittle in a number of ways. At very low temperatures some of the Fe-based alloys break brittly. Some compositions (high metalloid, Ca-based alloys, etc.) are brittle as-made [80]. Most important, however, is the brittleness caused by annealing at intermediate temperatures ($T \approx T_g - 100$ K). Some alloys, mainly the Fe- and other b.c.c.-based ones, become brittle this way [81]. Other amorphous alloys, however, such as Pd_4Si or CuZr, have been annealed at these temperatures and do not experience any embrittling. It has also been shown that the brittleness can be reversed: irradiation of brittle $(Mo_{0.6}Ru_{0.4})_{82}B_{18}$ with neutrons makes it ductile [44].

A theoretical understanding of the embrittling phenomenon has not yet developed. Some workers [82, 83] attribute it, on indirect experimental grounds, to separation of the amorphous metal into two amorphous phases with different composition. However, a $Pd_{74}Au_8Si_{18}$ alloy, for which the amorphous phase separation phenomenon has been clearly established [84] does not exhibit any embrittlement upon separation. Furthermore, separation *per se* does not yet explain why one of the phases would then be brittle.

Another school of thought [85] is based on the large viscosity increase which is known to occur upon annealing below T_g (see subsection 3.2.1). Such an increase could make flow at the crack tip more difficult, and hence prevent the plastic flow necessary to forestall cleavage. The problem with this approach is that it is too general. $Pd_{82}Si_{18}$ is a system for which the viscosity increase is best documented [51]; however, it does not embrittle at all, even after hundreds of annealing hours. Also, from a mechanistic point of view, the dilatation model for shear band nucleation discussed above (subsection 4.3.1) seems powerful enough to overcome a large viscosity increase upon annealing.

The answer to the embrittling problem has probably several aspects. One of them is chemical, given the large differences in behavior for different classes of amorphous metals. The other one is a proper adaption of the approach involving the viscosity increase. There is no doubt that this increase is important, especially given the reverse phenomenon, the elimination of brittleness by irradiation, which, presumably, produces an increase in free volume and a lowering of the viscosity. To illuminate this question a detailed fracture mechanics analysis of the competition between shear band formation and cleavage, taking into account the time dependence of the viscosity changes, would be very desirable.

I would like to thank Prof. D. Turnbull for a critical reading of the manuscript. Our research in this area is supported by the Office of Naval Research, under Contract Number N00014-77-C-0002.

References

[1] Review of diffraction and structure: G. S. Cargill, III, in: Solid State Physics, eds. F. Seitz, D. Turnbull and H. Ehrenreich, Vol. 30 (Academic, New York, 1975) p. 227.
[2] General review: N. J. Grant and B. C. Giessen, eds., Proc. 2nd Int. Conf. on Rapidly Quenched Metals (MIT Press, Cambridge, MA, 1976).
[3] General review: B. Cantor, ed., Proc. 3rd Int. Conf. on Rapidly Quenched Metals, Vols. 1 and 2 (The Metal Society, London, 1978).
[4] General review: J. J. Gilman and H. J. Leamy, eds., Metallic Glasses, ASM Seminar (American Society for Metals, Metals Park, OH, 1976).
[5] General review: H. S. Chen, Rep. Prog. Phys. 43 (1980) 353.
[6] J. M. Poate, J. A. Borders, A. G. Cullis and J. K. Hirvonen, Appl. Phys. Lett. 30 (1977) 365.
[7] For a comparison of quenching and sputtering see, e.g. M. P. Rosenblum and D. Turnbull, J. Non-Cryst. Solids 37 (1980) 45.
[8] M. R. Bennett and J. G. Wright, Phys. Stat. Sol. A 13 (1972) 135; T. Ichikawa, Phys. Stat. Sol. A 19 (1973) 707.

[9] G. S. Cargill, III, J. Appl. Phys. 41 (1970) 12.
[10] J. D. Bernal, Nature 185 (1960) 68.
[11] J. L. Finney, Proc. R. Soc. A 319 (1970) 479.
[12] H. J. Frost, to appear in Acta Met.
[13] J. D. Bernal, Proc. R. Soc. A 280 (1964) 299.
[14] D. E. Polk, J. Non-Cryst. Solids 5 (1971) 365.
[15] P. Steinhardt, R. Alben and D. Weaire, J. Non-Cryst. Solids 15 (1974) 199.
[16] J. F. Sadoc and J. Dixmier, Mat. Sci. Eng. 23 (1976) 187.
[17] Y. Waseda, H. Okazaki and T. Masumoto, J. Mat. Sci. 12 (1977) 1927.
[18] T. M. Hayes, J. W. Allen, J. Tauc, B. C. Giessen and J. J. Hauser, Phys. Rev. Lett. 40 (1978) 1282.
[19] J. Wong, F. W. Lytle, R. B. Greegor, H. H. Liebermann, J. L. Walter and F. Luborsky, in ref. [3], Vol. 2, p. 345.
[20] S. Rundqvist, Acta Chem. Scand. 16 (1962) 242.
[21] P. H. Gaskell, J. Non-Cryst. Solids 32 (1979) 207.
[22] D. S. Boudreaux and J. M. Gregor, J. Appl. Phys. 48 (1977) 152; J. Appl. Phys. 48 (1977) 5057.
[23] G. S. Cargill, III and F. Spaepen, J. Non-Cryst. Solids 43 (1981) 91.
[24] M. H. Cohen and D. Turnbull, J. Chem. Phys. 31 (1959) 1164; D. Turnbull and M. H. Cohen, J. Chem. Phys. 34 (1961) 120; J. Chem. Phys. 52 (1970) 3038.
[25] M. R. Hoare, J. Non-Cryst. Solids 31 (1978) 157.
[26] F. Spaepen, Phil. Mag. 30 (1974) 417.
[27] F. Spaepen, J. Non-Cryst. Solids 31 (1978) 207.
[28] C. H. Bennett, P. Chaudhari, V. Moruzzi and P. Steinhardt, Phil. Mag. A 40 (1979) 485.
[29] P. D. Bristowe, A. Brokman, F. Spaepen and R. W. Balluffi, Scripta Met. 14 (1980) 943.
[30] H. J. Frost, M. F. Ashby and F. Spaepen, Scripta Met. 14 (1980) 1951.
[31] J. J. Gilman, J. Appl. Phys. 44, (1973) 675.
[32] J. C. M. Li, in ref. [4], p. 224.
[33] F. Spaepen, Acta Met. 25 (1977) 407.
[34] P. Chaudhari, A. Levi and P. Steinhardt, Phys. Rev. Lett. 43 (1979) 1517.
[35] S. Kobayashi, K. Maeda and S. Takeuchi, Acta Met. 28 (1980) 1641.
[36] H. S. Chen and S. Y. Chuang, J. Electr. Mater. 4 (1975) 783.
[37] E. Nold, S. Steeb and P. Lamparter, Phys. Lett. A, in press.
[38] T. Egami, K. Maeda and V. Vitek, Phil. Mag. A41 (1980) 883.
[39] D. Turnbull, J. Physique C-4 (1974) 1.
[40] B. J. Alder, D. M. Glass and T. E. Wainwright, J. Chem. Phys. 53 (1970) 3813.
[41] G. Adam and J. H. Gibbs, J. Chem. Phys. 43 (1965) 139.
[42] H. S. Chen, J. Non-Cryst. Solids 22 (1976) 135.
[43] H. S. Chen and D. Turnbull, J. Chem. Phys. 48 (1968) 2560.
[44] E. A. Kramer, W. L. Johnson and C. Cline, Appl. Phys. Lett. 35 (1979) 815.
[45] F. Spaepen and D. Turnbull, in ref. [4], p. 114.
[46] A. Q. Tool, J. Am. Ceram. Soc. 29 (1946) 240.
[47] D. E. Polk and D. Turnbull, Acta Met. 20 (1972) 493.
[48] H. S. Chen and M. Goldstein, J. Appl. Phys. 43 (1971) 1642.
[49] R. Maddin and T. Masumoto, Mat. Sci. Eng. 9 (1972) 153.
[50] J. Logan and M. F. Ashby, Acta Met. 22 (1974) 1047.

[51] A. I. Taub and F. Spaepen, Acta Met. 28 (1980) 1781.
[52] S. Glasstone, K. J. Laidler and H. Eyring, The theory of rate processes (McGraw Hill, New York, 1941) p. 480.
[53] H. S. Chen, J. Appl. Phys. 49 (1978) 3289.
[54] A. I. Taub, Acta Met. 28 (1980) 633.
[55] D. Gupta, K. N. Tu and K. W. Asai, Phys. Rev. Lett 35 (1975) 796.
[56] H. S. Chen, L. C. Kimerling, J. M. Poate and W. L. Brown, Appl. Phys. Lett. 32 (1978) 461.
[57] M. P. Rosenblum, F. Spaepen and D. Turnbull, Appl. Phys. Lett. 37 (1980) 184.
[58] H. E. Cook and J. E. Hilliard, J. Appl. Phys. 40 (1969) 2191.
[59] C. Birac and D. Lesueur, Phys. Stat. Sol. A 36 (1976) 247.
[60] R. W. Cahn, J. E. Evetts, J. Patterson, R. E. Somekh and C. K. Jackson, J. Mat. Sci. 15 (1980) 702.
[61] U. Köster and U. Herold, in: Metallic Glasses, ed. H. J. Güntherodt (Springer) in press.
[62] C. Herring, J. Appl. Phys. 21 (1950) 437.
[63] H. S. Chen, J. Non-Cryst. Solids 27 (1978) 257.
[64] M. F. Ashby, Acta Met. 20 (1972) 887.
[65] H. J. Frost and M. F. Ashby, Proc. John E. Dorn Symposium, eds. J. C. M. Li and A. K. Mukherjee (ASM, Metals Park, OH, 1975) p. 70.
[66] L. A. Davis, in ref. [4], p. 180.
[67] W. R. Tyson, Phil. Mag. 14 (1966) 925.
[68] T. Murata, T. Masumoto and M. Sakai, in ref. [3] Vol. 2, p. 401.
[69] C. A. Pampillo and D. E. Polk, Acta Met. 22 (1974) 741.
[70] H. Neuhäuser, Scripta Met. 12 (1978) 471.
[71] C. A. Pampillo, Scripta Met. 6 (1972) 915.
[72] T. Masumoto, H. Kimura, A. Inoue and Y. Waseda, Mat. Sci. Eng. 23 (1976) 141.
[73] F. Spaepen and D. Turnbull, Scripta Met. 8 (1974) 563.
[74] A. S. Argon, Acta Met. 27 (1979) 47.
[75] P. G. Saffman and G. I. Taylor, Proc. R. Soc. London A 245 (1958) 312.
[76] F. Spaepen, Acta. Met. 23 (1975) 615.
[77] A. S. Argon and M. Salama, Mat. Sci. Eng. 23 (1976) 219.
[78] E. Pitts and J. Greiller, J. Fluid Mech. 11 (1961) 33.
[79] W. W. Mullins and R. F. Sekerka, J. Appl. Phys. 35 (1964) 444.
[80] H. S. Chen and D. E. Polk, J. Non-Cryst. Solids 15 (1974) 174.
[81] F. E. Luborsky and J. L. Walter, J. Appl. Phys. 47 (1976) 3648.
[82] H. S. Chen, Scripta Met. 11 (1977) 367.
[83] J. L. Walter, F. Bacon and F. Luborsky, Mat. Sci. Eng. 24 (1976) 239.
[84] C. P. Chou and D. Turnbull, J. Non-Cryst. Solids 17 (1975) 168.
[85] R. S. Williams and T. Egami, in ref. [3], Vol. 1, p. 214.
[86] W. Kauzmann, Chem. Rev. 42 (1948) 219.

Defense Documentation Center
Cameron Station
Alexandria, Virginia 22314 (12)

Office of Naval Research
Department of the Navy
Attn: Code 471 (3)
Code 105 (6)
Code 470

Director
Office of Naval Research
Branch Office
495 Summer Street
Boston, Massachusetts 02210

Director
Office of Naval Research
Branch Office
536 South Clark Street
Chicago, Illinois 60605

Office of Naval Research
San Francisco Area Office
760 Market Street, Room 447
San Francisco, California 94102

Naval Research Laboratory
Washington, D.C. 20390
Attn: Code 6000
Code 6100
Code 6300
Code 6400
Code 2627 (6)

Attn: Mr. F S Williams
Naval Air Development Center
Code 302
Warminster, Pennsylvania 18974

Naval Air Propulsion Test Center
Trenton, New Jersey 08628
Attn: Library

Naval Weapons Laboratory
Dahlgren, Virginia 22448
Attn: Research Division

Naval Construction Battalion
Civil Engineering Laboratory
Port Hueneme, California 93041
Attn: Materials Division

Naval Electronics Laboratory Center
San Diego, California 92152
Attn: Electronic Materials Sciences Div.

Naval Missile Center
Materials Consultant
Code 3312-1
Point Mugu, California 93041

Commanding Officer
Naval Ordnance Laboratory
White Oak
Silver Spring, Maryland 20910
Attn: Library

Naval Ship R and D Center
Materials Department
Annapolis, Maryland 21402

Naval Undersea Center
San Diego, California 92132
Attn: Library

Naval Underwater System Center
Newport, Rhode Island 02840
Attn: Library

Naval Weapons Center
China Lake, California 93555
Attn: Library

Naval Postgraduate School
Monterey, California 93940
Attn: Materials Sciences Dept.

Naval Air Systems Command
Washington, D.C. 20360
Attn: Code 52031
Code 52032
Code 320

Naval Sea System Command
Washington, D.C. 20362
Attn: Code 035

Naval Facilities
Engineering Command
Alexandria, Virginia 22331
Attn: Code 03

Scientific Advisor
Commandant of the Marine Corps
Washington, D.C. 20380
Attn: Code AX

Naval Ship Engineering Center
Department of the Navy
Washington, D.C. 20360
Attn: Director, Materials Sciences

Army Research Office
Box CM, Duke Station
Durham, North Carolina 27706
Attn: Metallurgy and Ceramics Div

Army Materials and Mechanics
Research Center
Watertown, Massachusetts 02172
Attn: Res Programs Office (AMXMR-PR

Commanding General
Department of the Army
Frankford Arsenal
Philadelphia, Pennsylvania 19137
Attn: ORDBA-1320

Office of Scientific Research
Department of the Air Force
Washington, D.C. 20333
Attn: Solid State Div (SRPS)

Aerospace Research Labs
Wright-Patterson AFB
Building 450
Dayton, Ohio 45433

Air Force Materials Lab (LA)
Wright-Patterson AFB
Dayton, Ohio 45433

NASA Headquarters
Washington, D.C. 20546
Attn: Code RRM

NASA
Lewis Research Center
21000 Brookpark Road
Cleveland, Ohio 44135
Attn: Library

National Bureau of Standards
Washington, D.C. 20234
Attn: Metallurgy Division
Inorganic Materials Division

Atomic Energy Commission
Washington, D.C. 20545
Attn: Metals and Materials Branch

Defense Metals and Ceramics
Information Center
Battelle Memorial Institute
505 King Avenue
Columbus, Ohio 43201

Director
Ordnance Research Laboratory
P.O. Box 30
State College, Pennsylvania 16801

Director Applied Physics Lab.
University of Washington
1013 Northeast Forty-Third Street
Seattle, Washington 98105

Metals and Ceramics Division
Oak Ridge National Laboratory
P.O. Box X
Oak Ridge, Tennessee 37830

Los Alamos Scientific Lab.
P.O. Box 1663
Los Alamos, New Mexico 87544
Attn: Report Librarian

Argonne National Laboratory
Metallurgy Division
P.O. Box 229
Lemont, Illinois 60439

Brookhaven National Laboratory
Technical Information Division
Upton, Long Island
New York 11973
Attn: Research Library

Library
Building 50, Room 134
Lawrence Radiation Laboratory
Berkeley, California

Professor G.S. Ansell
Rensselaer Polytechnic Institute
Dept. of Metallurgical Engineering
Troy, New York 12181

Professor H.K. Birnbaum
University of Illinois
Department of Metallurgy
Urbana, Illinois 61801

Dr. E.M. Breinan
United Aircraft Corporation
United Aircraft Research Lab
East Hartford, Connecticut 06108

Professor H.D. Brody
University of Pittsburgh
School of Engineering
Pittsburgh, Pennsylvania 15213

Professor J.B. Cohen
Northwestern University
Dept. of Material Sciences
Evanston, Illinois 60201

Professor M. Cohen
Massachusetts Institute of Technology
Department of Metallurgy
Cambridge, Massachusetts 02139

Professor B.C. Giessen
Northeastern University
Department of Chemistry
Boston, Massachusetts 02115

Dr. G.T. Hahn
Battelle Memorial Institute
Department of Metallurgy
505 King Avenue
Columbus, Ohio 43201

Professor P.W. Hoper
Carnegie-Mellon University
Research Park
Pittsburgh, Pennsylvania 15213

Dr. David G. Howden
Battelle Memorial Institute
Columbus Laboratories
505 King Avenue
Columbus, Ohio 43201

Professor C.E. Jacobson
Ohio State University
Dept. of Welding Engineering
190 West 19th Avenue
Columbus, Ohio 43210

Professor G. Judd
Rensselaer Polytechnic Institute
Dept. of Materials Engineering
Troy, New York 12181

Dr. C.S. Kortovich
TRW, Inc.
23555 Euclid Avenue
Cleveland, Ohio 44117

Professor D.A. Koss
Michigan Technological University
College of Engineering
Houghton, Michigan 49931

Professor A. Lawley
Drexel University
Dept. of Metallurgical Engineering
Philadelphia, Pennsylvania 19104

Dr. H. Margolin
Polytechnic Institute of New York
333 Jay Street
Brooklyn, New York 11201

Professor K. Masubuchi
Massachusetts Institute of Technology
Department of Ocean Engineering
Cambridge, Massachusetts 02139

Dr. G.H. Meier
University of Pittsburgh
Dept. of Metallurgical and Materials
Engineering
Pittsburgh, Pennsylvania 15213

Professor J.W. Morris, Jr.
University of California
College of Engineering
Berkeley, California 94720

Professor K. Ono
University of California
Materials Department
Los Angeles, California 90024

Professor W.F. Savage
Rensselaer Polytechnic Institute
School of Engineering
Troy, New York 12181

Dr. C. Shaw
Rockwell International Corp.
P.O. Box 1259
1049 Camino Dos Rios
Thousand Oaks, California 91360

Professor O.D. Sherby
Stanford University
Materials Science Dept.
Stanford, California 94305

Professor J. Shyne
Stanford University
Materials Sciences Department
Stanford, California 94305

Dr. W.A. Spitzig
U.S. Steel Corporation
Research Laboratory
Monroeville, Pennsylvania 15146

Dr. E.A. Starke, Jr.
Georgia Institute of Technology
School of Chemical Engineering
Atlanta, Georgia 30332

Professor N.S. Stoloff
Rensselaer Polytechnic Institute
School of Engineering
Troy, New York 12181

Dr. E.R. Thompson
United Aircraft Research Lab
400 Main Street
East Hartford, Connecticut 06108

Professor David Turnbull
Harvard University
Division of Engineering and Applied
Physics
Cambridge, Massachusetts 02139

Dr. F.W. Wang
Naval Ordnance Laboratory
Physics Laboratory
White Oak
Silver Spring, Maryland 20910

Dr. J.C. Williams
Rockwell International
Science Center
P.O. Box 1085
Thousand Oaks, California 91360

Professor H.G.F. Wilsdorf
University of Virginia
Department of Materials Science
Charlottesville, Virginia 22901

Dr. L.A. Wood
National Bureau of Standards
Space Institute
Dept. of Metallurgical Engineering
Tullahoma, Tennessee 37388